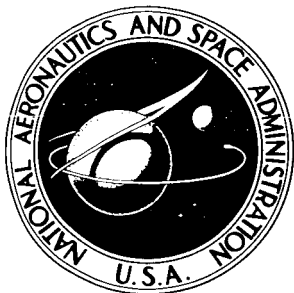# NASA TECHNICAL NOTE

NASA TN D-3905

NASA TN D-3905

GPO PRICE $ _____

CFSTI PRICE(S) $ ___3.00_____

Hard Copy (HC) _____

Microfiche (MF) _____

ff 653 July 65

TUNNEL DIODE LOW-LEVEL DETECTION

by W. F. Gabriel

Goddard Space Flight Center
Greenbelt, Md.

NATIONAL AERONAUTICS AND SPACE ADMINISTRATION • WASHINGTON, D. C. • JUNE 1967

TUNNEL DIODE LOW-LEVEL DETECTION

By W. F. Gabriel

Goddard Space Flight Center
Greenbelt, Md.

NATIONAL AERONAUTICS AND SPACE ADMINISTRATION

ABSTRACT

An analysis of tunnel diode low-level detection is presented for the purpose of explaining some of the unusual detection characteristics that occur under certain bias conditions. For example, in the vicinity of its inflection bias point, a tunnel diode exhibits a discriminator-like rectification behavior with two sensitivity peaks. When biased at one of these peaks, the diode is capable of unusually high sensitivities, at least an order of magnitude better than the sensitivity of any other known diode. It is shown that these high sensitivities are proportional to $(1-\Gamma^2)$, where Γ^2 is the RF power gain of the detector viewed as a reflection-type amplifier. The resultant gain-bandwidth (or sensitivity-bandwidth) limitations of the detector are discussed. Unusually high sensitivities are also possible at the lower microwave frequencies when the tunnel diode is biased at its peak current point.

A knowledge of the diode static characteristics, the reflection coefficient, and the video circuit permits an accurate analytical evaluation of the sensitivity performance of any tunnel diode, and calculations are carried out for an example diode and compared against measured data. This report also contains a specific comparison of the relative sensitivity performance of the example tunnel diode vs. a hot carrier diode.

CONTENTS

TUNNEL DIODE LOW-LEVEL DETECTION

by
W. F. Gabriel
Goddard Space Flight Center

INTRODUCTION

Microwave low-level detection, which was entirely dependent upon the rather unpredictable silicon point-contact crystal rectifier (Reference 1) for so many years, has been advanced considerably by the development of tunnel diode (or back diode) detectors and hot carrier diode detectors. Both of these solid junction devices have demonstrated advantages of lower noise (particularly 1/f noise), higher rectification current sensitivity, low temperature variation, high burn-out capability, high resistance to noise impulse generation under shock and vibration, aging stability, broad bandwidth capability, and accurate analytical performance evaluation from measured static characteristics.

The excellent performance of the hot carrier diode under bias conditions has been reported in the literature (References 2 and 3), together with an adequate analysis. In the case of the tunnel diode, however, despite numerous references (References 4 to 10) reporting on specific examples of sensitivity performance, the analyses are found to be restricted and incomplete such that important features of the overall behavior of this versatile detector are overlooked. For instance, it is not generally appreciated that the tunnel diode, when biased in its negative resistance region, is capable of at least an order of magnitude greater sensitivity than any other diode detector for frequencies below resistive cutoff. Also, that it is capable of bi-polar amplitude modulation of its video output. The former capability can be of considerable advantage in sensitive TRF (tuned radio frequency) receivers (References 11 and 12) such as those employed in compact solid-state transponders for missiles, spacecraft, and aircraft.

The purpose of this report is to present a low-level detector analysis which is general enough to cover tunnel diode behavior for any bias condition, and to demonstrate detection features which are peculiar to the tunnel diode. Super-regenerative detection and converter action are not included in this discussion; i.e., the tunnel diode detector circuit is assumed to be in a stable condition at all times.

In the work described herein, the rectification current sensitivity, β, is expressed as a function of the reflection coefficient, Γ. It is shown that a knowledge of this quantity, together with the diode static characteristics and the video circuit, permits accurate analysis of low-level detection performance for any bias condition. Calculations are carried through on an example diode and compared against measured data.

When a tunnel diode detector is biased in its negative resistance region and operated below resistive cutoff frequency, it is an RF amplifier and must look into an impedance that insures stable operation; i.e., it requires a non-reciprocal isolator or circulator to insure stability against spurious oscillations. As an amplifier, it exhibits the usual gain-bandwidth limitations. Examples of sensitivity behavior versus RF bandwidth are also discussed.

The final section of the report discusses diode figure of merit, M, and here a specific comparison with the hot carrier diode is made in order to illustrate relative sensitivity capability.

EQUIVALENT CIRCUIT AND DIODE CHARACTERISTICS

Microwave low-level detectors usually consist of a combination of transmission line circuits and lumped reactances, plus the diode. The complete detailed equivalent circuit can be quite complicated, particularly in the case of broadband designs, but for the purposes of the present analytical discussion it is preferably to reduce it to the simple equivalent circuit shown in Figure 1. This circuit is referenced to the diode junction and is often utilized for diode analysis (References 13 to 17). Circuit elements R_g and L are both functions of frequency since they represent the series equivalent of the impedance that includes the diode series inductance, the diode package capacitance, and the entire external RF input circuit.
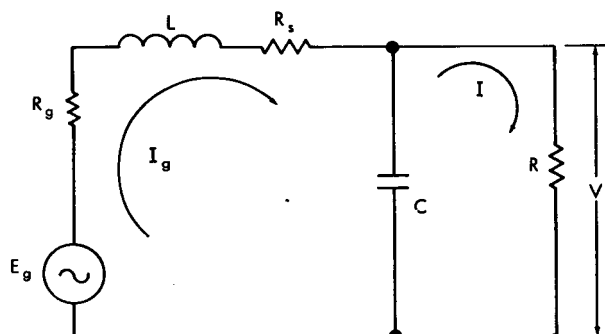
R - DIFFERENTIAL JUNCTION RESISTANCE, (dV/dI), OF DIODE

C - JUNCTION CAPACITANCE OF DIODE

R_s - SERIES RESISTANCE OF DIODE

L - EQUIVALENT RF CIRCUIT PLUS DIODE SERIES INDUCTANCE

R_g - EQUIVALENT RF CIRCUIT RESISTANCE

Figure 1—Equivalent circuit of detector referred to diode junction.

The differential junction resistance, R, may assume either positive or negative values. When it is negative, the circuit represents a negative-resistance reflection-type amplifier where the voltage gain is simply equal to the reflection coefficient, Γ, referred to R_g, i.e.,

$$\Gamma = \frac{(Z - R_g) - R_g}{(Z - R_g) + R_g} = \frac{Z - 2R_g}{Z} \quad , \qquad (1)$$

where Z is the total series impedance of the circuit.

$$Z = \left[R_g + R_s + \frac{R}{1 + (\omega CR)^2} \right] + j \left[\omega L - \frac{R(\omega CR)}{1 + (\omega CR)^2} \right] . \qquad (2)$$

This type of tunnel diode amplifier and its stability considerations are widely discussed in the literature (References 13 to 21). Circuit stability criteria must be satisfied at all frequencies below the resistive cutoff frequency in order to insure finite values for Γ and avoid spurious oscillation

2

For Figure 1, a safe and sufficient (Reference 18) stability criterion* may be written in the form,

$$|R| > (R_s + R_g) > \frac{L}{|R|C} \text{ for negative } R .$$ (3)

A small-signal analysis of the Figure 1 circuit is carried out in Appendix A for the purpose of deriving a general expression for β. This shows that the basic diode quantities required are G, R_s, C, and G', where G' is the first derivative of the diode differential junction conductance, G. (Note that G is the reciprocal of R, so that the determination of either quantity is sufficient. Both will be utilized freely in accordance with their convenience to the discussion.) Of these quantities, all except C can be evaluated from the measured static V-I (voltage-current) characteristic. For purposes of practical illustration and experimental confirmation, the measured characteristics of an actual diode example, a selected MS-1012 back diode, will be utilized throughout the discussion.

A back diode (Reference 21) or "backward diode," as they are sometimes called, is simply a tunnel diode with a low peak current wherein the "forward voltage" direction is reversed (backwards) from the usual tunnel diode polarity. This reversed presentation happens to be very convenient for comparison with other types of diode detectors because it results in the same direction of rectified current flow for typical bias conditions, and so it will be utilized throughout this report. Figure 2 illustrates the V-I characteristic of the example diode and also that of a typical hot carrier diode. Three distinct bias points, labelled "o", "p", and "i", are denoted on the back diode curve because (1) they are often referred to throughout the report and (2) they are frequently used as subscripts on the voltage and current;

"o" - refers to the diode zero bias point,

"p" - refers to the diode peak current bias point,

"i" - refers to the diode inflection bias point.

Although the low peak current ($I_p = -0.286$ma) qualifies the example diode to be called a back diode, it will be referred to as a tunnel diode throughout this report because (1) it has a
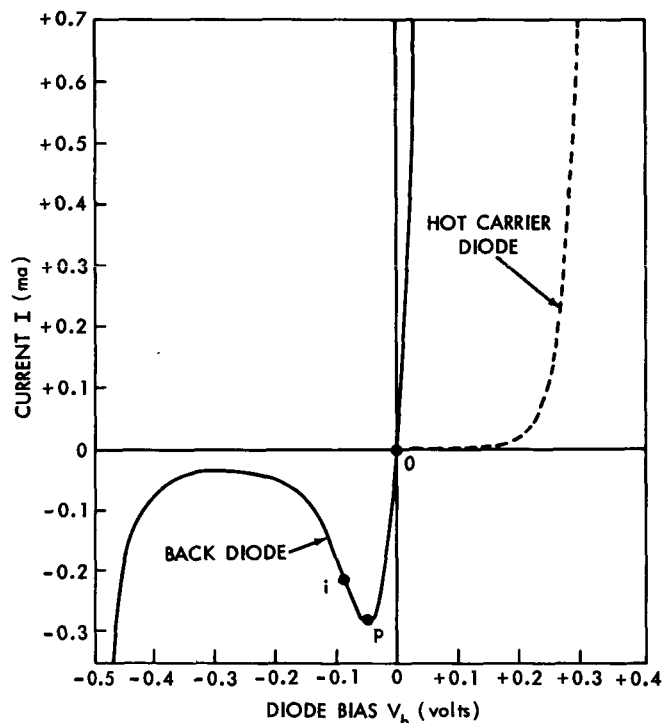

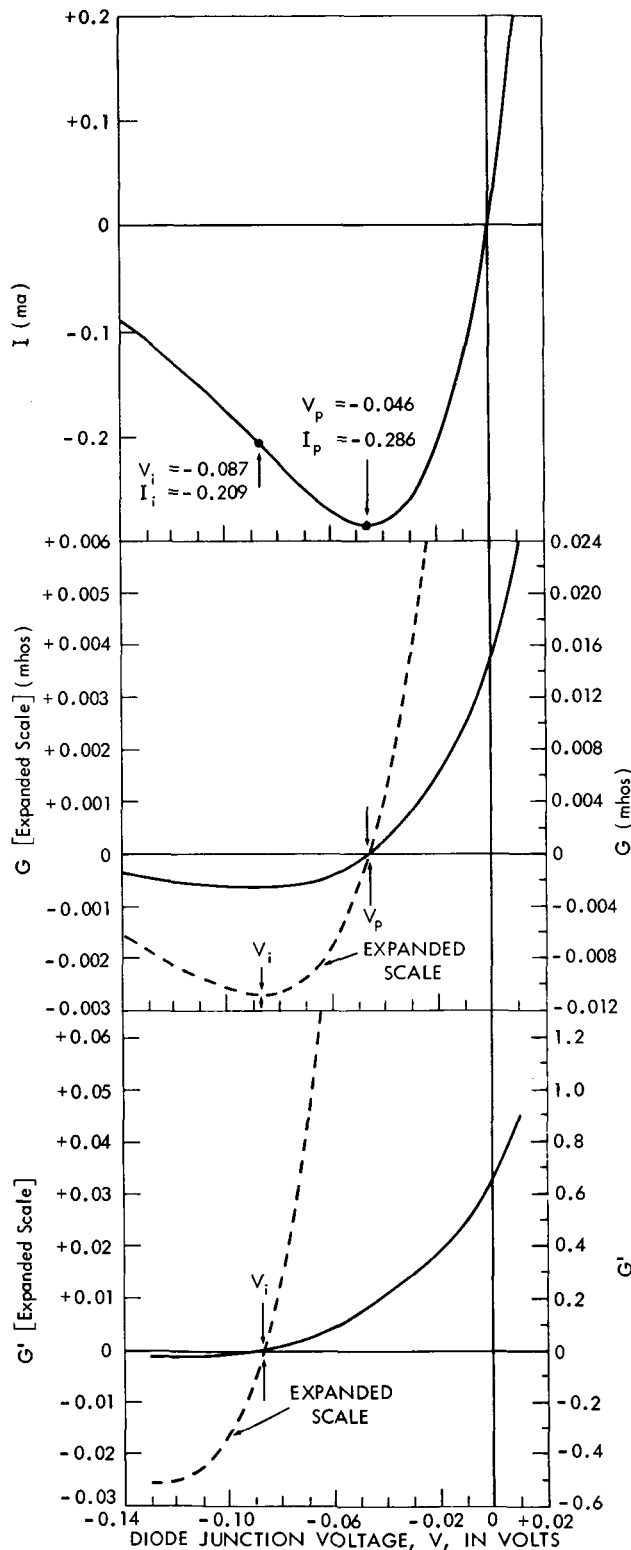Figure 2—Static voltage–current characteristics for example diode (MS-1012) and a hot carrier diode (hpa-2350) at 25°C.

Figure 3—Static characteristics vs. diode junction voltage, V: (a) Current I, vs. V, (b) Differential junction conductance, G vs. V, (c) First derivative of G, G′, vs. V.

resistive cut-off frequency of about 9 Gc, and, (2) it was chosen specifically to demonstrate the detection behavior that can be obtained when biased into the negative resistance region.

A calculation of the derivatives, G and G′ from Figure 2 requires an analytical expression for the tunnel diode current. This problem is treated in Appendix B, and the results are plotted in Figure 3 for the diode voltage range of greatest interest. Note that the voltage scale in Figure 3 is the diode junction voltage instead of the diode bias voltage; i.e.,

$$V_b = V + I R_s , \qquad (4)$$

where V is the internal junction voltage and V_b is the external bias voltage across the diode terminals. The junction voltage is required for the calculations. The expressions G and G′ for a tunnel diode behave in a different manner than the similar derivatives of a hot carrier or point contact diode in that they do not bear a constant ratio to one another, they do have a zero point, and they can assume negative values as well as positive values.

The diode series resistance, R_s, can be found from the forward conduction characteristic (a standard technique) as described in Appendix B, if it is not given as part of the manufacturer's data. A value of 8 ohms for R_s was measured on the example diode with an estimated accuracy of 5 percent.

Diode junction capacitance C must be measured if not given by the manufacturer. Applicable measurement techniques include the familiar RF bridge (Reference 22) method, microwave impedance determination, or resistive cut-off frequency determination. For the example diode, the latter approach was employed. The resistive cut-off frequency, f_r, occurs at

4

the point where the equivalent series resistance of the diode goes to zero, and it is readily shown that

$$f_r = \frac{\sqrt{\frac{|R|}{R_s} - 1}}{2\pi C |R|} \quad \text{for negative R .} \tag{5}$$

Since the total series resistance is zero at f_r, it follows that the diode will look like a short circuit at resonance whereby $\Gamma = -1$. Thus, the technique consists of tuning the detector to resonance at any convenient microwave frequency, and recording the bias voltage required to give a reflection coefficient exactly equal to unity at that frequency. The frequency thereby becomes an f_r value; R_s is known; R can be determined from Figure 3b since the bias voltage is known; and this then permits solving for C from Equation 5. A value of 0.3 picofarads was arrived at for the example diode via this technique.

The f_r technique is easy to implement and use, and it has a great advantage in that it is independent of the diode package capacitance.

RECTIFICATION CURRENT SENSITIVITY, β

The rectification current sensitivity, β, is defined as the ratio of the detector rectified output current, I_r, to the RF power, P_i, incident upon the detector, or

$$I_r = \beta P_i . \tag{6}$$

A general equation for β is derived in Appendix A on the basis of a small-signal analysis of the detector equivalent circuit shown in Figure 1,

$$\beta = \frac{2G' R_g |Z_j|^2}{(1 + G R_s) |Z|^2} , \tag{7}$$

where

$$Z_j = \frac{1}{G + j \omega C} , \tag{8}$$

and Z is given by Equation 2. Equation 7 holds for either positive or negative values of G, subject to the restriction that the tunnel diode circuit be stable. An inspection of the various terms in Equation 7 shows that β will vary principally as a function of three parameters:

(a) diode bias voltage

(b) equivalent source resistance, R_g

(c) frequency

A variation in the diode bias voltage causes a variation in G and G' as illustrated in Figure 3. Junction capacitance, C, also changes with bias, (Reference 15) but the effect is of minor importance compared to G and G'.

R_g determines the reflection coefficient, Γ, as given by Equation 1.* Because of the familiar interpretation of Γ for tunnel diodes and the fact that it is a readily measured microwave quantity, it becomes desirable to convert the series impedance, Z, in Equation 7 to Γ. Solving for Z from Equation 1 results in,

$$Z = \left(\frac{2R_g}{1-\Gamma} \right) ,$$

(9)

and substituting this into (7) permits β to be written as

$$\beta = \frac{G' \cdot |(1-\Gamma)|^2}{2R_g(1+GR_s)[G^2+(\omega C)^2]}.$$

(10)

It will be noted that β can increase almost in direct proportion to the RF power gain, $|\Gamma|^2$, of the tunnel diode, thus indicating the possibility of very large current sensitivities.

Equation 10 can be manipulated into several interesting forms by applying appropriate restrictions upon Γ and G. If we apply the restriction that Γ be real (circuit resonance condition), then from Equations 2 and 1:

$$Z = R_g + R_s + r ,$$

(11)

and

$$\Gamma = \frac{R_s + r - R_g}{R_s + r + R_g} ,$$

(12)

where

$$r = \frac{R}{1+(\omega CR)^2} .$$

(13)

r is the equivalent series resistance of the diode junction. Solving for R_g from Equation 12 and substituting into Equation 10 results in

$$\beta_1 = \beta_0 \left[\frac{(1-\Gamma^2)}{1+\left(\dfrac{R_s(\omega CR)^2}{R+R_s} \right)} \right] \qquad \begin{array}{l} \text{Restrictions:} \\ \Gamma \text{ is real} \end{array}$$

(14)

---

*This interpretation is dependent upon R_g representing only the generator source resistance. If R_g includes any loss components, then Equation 1 and Equation 7 must be corrected to incorporate the loss factor.

where

$$\beta_0 = \frac{G'}{2G(1 + GR_s)^2} \quad . \tag{15}$$

If we next restrict G to positive values only, then Equation 14 may be written as,

$$\beta_2 = \beta_0 \left[\frac{1 - \Gamma^2}{1 + \left(\frac{f}{f_c}\right)^2} \right] \qquad \begin{array}{l} \text{Restrictions:} \\ \Gamma \text{ is real} \\ G \text{ is positive} \end{array} \tag{16}$$

where

$$f_c = \frac{\sqrt{\left(\frac{R}{R_s}\right) + 1}}{2\pi C R} \quad . \tag{17}$$

Equation 16 applies to hot carrier and point contact diodes as well as tunnel diodes. The frequency f_c is the usual "cutoff" frequency defined for diodes. For a positive G, $|\Gamma| \leq 1$, so that the optimum value of β_2 occurs for matched conditions, i.e., $\Gamma = 0$, whereupon Equation 16 becomes identical to the usual current sensitivity expressions found in the literature (References 1 and 3).

A special form for β occurs when we impose the restriction of biasing the tunnel diode at its peak current point (I_p, V_p) where G goes to zero. From Equations 9, 10, and 11 one obtains the simple expression

$$\beta_p = \frac{G'(1 - \Gamma^2)}{2 R_s (\omega C)^2} . \qquad \begin{array}{l} \text{Restrictions:} \\ \Gamma \text{ is real} \\ G \text{ is zero} \end{array} \tag{18}$$

Like β_2 above, β_p is optimized for $\Gamma = 0$.

If we restrict G to negative values only, then Equation 14 may be written as

$$\beta_3 = \beta_0 \left[\frac{1 - \Gamma^2}{1 - \left(\frac{f}{f_r}\right)^2} \right] \qquad \begin{array}{l} \text{Restrictions:} \\ \Gamma \text{ is real} \\ G \text{ is negative} \end{array} \tag{19}$$

where

$$f_r = \frac{\sqrt{\frac{|R|}{R_s} - 1}}{2\pi C |R|} \quad , \tag{20}$$

the frequency f_r will be recognized as the resistive cutoff frequency of a tunnel diode, above which the diode cannot supply RF gain; i.e., $|\Gamma| < 1$ for $f > f_r$. It follows that for $f > f_r$, β_3 will be optimized when $\Gamma = 0$.

When $f = f_r$, the β_3 expression becomes indeterminant and one must go back to the general Equation 10 to compute β, utilizing the fact that $\Gamma = -1$ for this particular condition.

Finally, when $f < f_r$, Equation 12 shows that $|\Gamma| > 1$ and may be made arbitrarily large by adjusting R_g, so that no optimum value for β_3 can be defined and it may be increased without limit, at least in theory.

A plot of the two frequencies, f_c and f_r, vs. bias for our example tunnel diode is shown in Figure 4. Knowing these values, it is then a simple matter to compute the gross frequency behavior of β from Equations 16 or 19 for a given Γ. The data points shown in Figure 4 were the frequencies at which f_r measurements were made in order to determine the value of the diode junction capacitance (refer back to pages 4 and 5 for description of measurement).

Figure 5 illustrates the gross frequency behavior of β for the example diode under various bias conditions and specified values of Γ. The optimum curves for zero bias, $V = -0.02$ volts, and $V = -0.04$ volts are calculated from Equation 16 since G is positive, and the $(\beta_0\, f_c)$ product tends to be constant for these positive conductance bias conditions. The zero bias curve shows good sensitivity capability in the millimeter-wave frequency region.

The optimum curve for the peak current bias point, $V_p = -0.046$ volts, is calculated from Equation 18 since G is zero, and it demonstrates the unique 6 db per octave constant slope obtained for
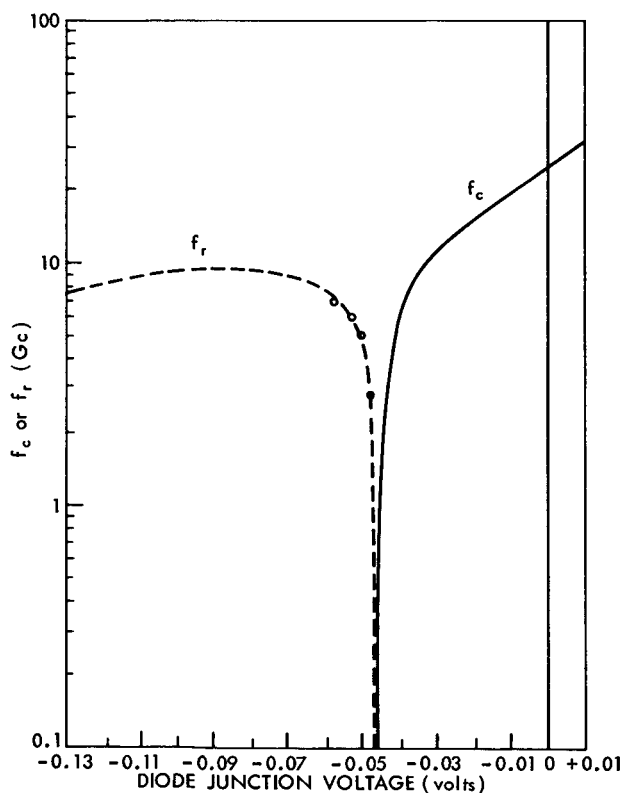
Figure 4—f_c and f_r versus junction
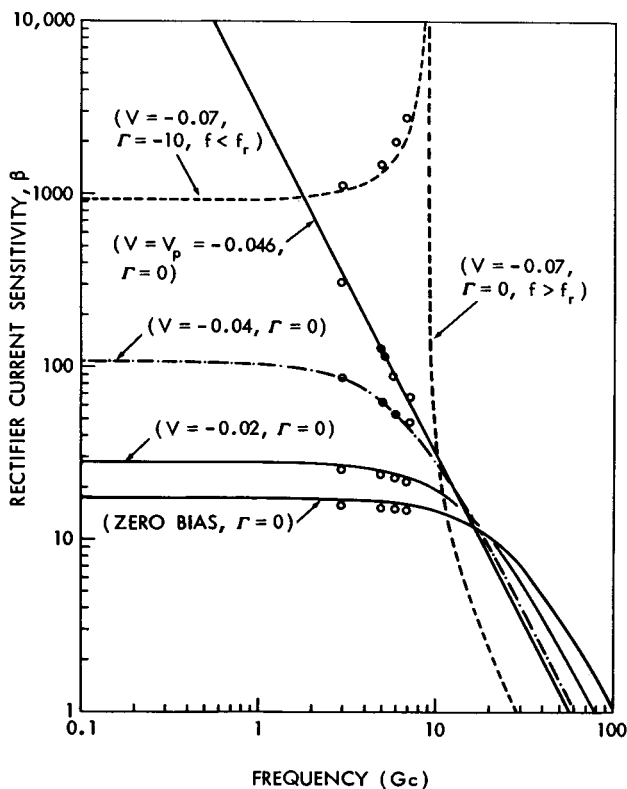voltage for example diode.

Figure 5—Gross frequency behavior of β for example
diode at various bias conditions and specified values of Γ.

this particular bias condition. Note that this constant slope behavior results in unusually high sensitivities at the lower microwave frequencies, and full advantage may be taken of this if the circuit losses can be kept small; i.e., the detector circuit Q is inversely proportional to frequency $(Q = 1/2 \: \omega CR_s)$ for the V_p bias condition.

The dashed-line curve for $V = -0.07$ volts, $\Gamma = -10$, and $f < f_r$ is calculated from Equation 19 since G is negative, and it clearly shows the high sensitivities that can be obtained at microwave frequencies below resistive cut-off when a tunnel diode is biased in its negative resistance region. An interesting feature of this curve is that β tends to approach infinity as the frequency approaches f_r. This behavior is simply the result of assuming a constant value for Γ, whereby the circuit Q would increase rapidly as f_r was approached. In actual practice, an operation close to f_r requires such low generator impedances to maintain a given value of Γ that coupling circuit losses become important and the resultant attenuation of the incident RF power must be taken into account.

The importance of f_r in tunnel diode detection cannot be emphasized too strongly, because detection sensitivity drops rather abruptly beyond f_r and results in poor sensitivity performance. This behavior is illustrated by the dashed-line optimum curve for $V = -0.07$ volts, $f > f_r$ which is also calculated from Equation 19. Note that this curve drops below the zero bias curve by a factor of about ten in the millimeter wave region.

The calculated curves of Figure 5 have been experimentally verified for the example diode at spot frequencies of 3, 5, 6, and 7 Gc. Experimental confirmation at many other values of Γ was also obtained, but the data has been omitted in the interest of keeping the family of curves as simple as possible.

From Figure 5 it is evident that there must be a continuous variation in β vs. bias under stable operating conditions, and a typical example of this type of variation is illustrated in Figure 6(a) for the example diode. The solid curve was calculated from Equation 10 under the conditions of $R_g = 85$ ohms and detector circuit resonance at 3 Gc. Note the bipolar behavior of β caused by the change in sign of G' as the diode is biased through the inflection point (Figure 3). The tunnel diode changes its direction of rectification when biased beyond the inflection point. Figure 6(b) illustrates the associated variation in $|\Gamma|^2$ vs. bias, which demonstrates the fact that rectification passes through zero at the peak RF gain point (under single-tuned conditions). This rectification reversal results in a discriminator-like characteristic with two sensitivity peaks, one above and one below the inflection bias point. The upper peak point has the highest sensitivity and is generally utilized as the operating bias point for high-sensitivity detectors. Practical bias adjustment procedure consists of "rocking" the bias back and forth to find the maximum video output point.

The discriminator-like characteristic can be utilized for bipolar amplitude modulation of output video signals via bias voltage control. This property would be useful, for example, in feedback control of tunnel diode amplifier operating bias point.

Experimental data points measured at 3 Gc for the assumed conditions are also shown plotted in Figure 6. The equivalent generator impedance of 85 ohms was initially approximated by adjusting the detector for an RF power gain of 15.6 db (calculated from Equation 12 for $R_g = 85\Omega$) with the diode

biased at its inflection point. The discrepancies between the measured data and calculated curves appear reasonable in view of the R_g approximation plus expected error in the values of G, G', and C.

As a practical note, it should be pointed out that the zero rectification point provides an extremely sensitive means for locating the exact inflection point on a tunnel diode characteristic.

BANDWIDTH BEHAVIOR OF β

The gross frequency behavior of β shown in Figure 5 was determined on the basis of constant values of Γ for all frequencies. If Γ could be so maintained, then by Equation 16 a maximum β-bandwidth product equal to $(\beta_0 \, f_c)$ would exist when the diode is biased in the positive conductance region, and by Equation 19 a product in excess of $(\beta_0 \, f_r \, (1 - \Gamma^2))$ would exist when the diode is biased in the negative conductance region. However, practical detector mounts cannot be designed to maintain Γ constant over the frequency range plotted in Figure 5, therefore actual β-bandwidth products are always less than the above values.

In general, bandwidth will be inversely proportional to the Q factor of the equivalent circuit shown in Figure 1, which may be written

$$Q = \left(\frac{\omega_0 L}{R_g + R_s + r_0} \right) , \qquad (21)$$

where

$$r_0 = \frac{R}{1 + (\omega_0 CR)^2} . \qquad (22)$$

ω_0 is taken to be the center frequency of the passband and r_0 is the equivalent series resistance of the diode junction at ω_0. For purposes of illustration, it is convenient to calculate the simple case of fixed element,
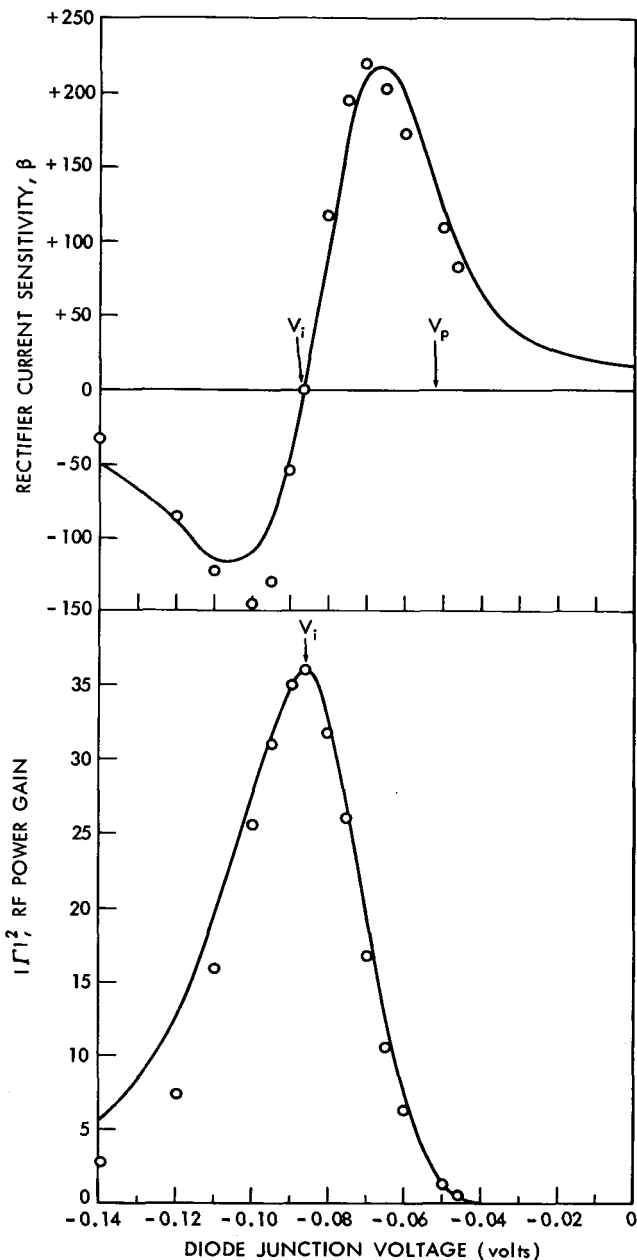

Figure 6—β and $|\Gamma|^2$ versus junction voltage for example diode under conditions of R_g = 85 ohms and detector circuit resonance at 3 Gc: (a) β vs. diode junction voltage, (b) $|\Gamma|^2$ vs. diode junction voltage.

10

single-tuned, series resonance* wherein the bandwidth, Δf, is given by the familiar ratio of f_0/Q, so that from Equation 21 obtains,

$$\Delta f = \frac{f_0}{Q} = \frac{R_g + R_s + r_0}{2\pi L} \quad .$$ (23)

Upon substituting for L from the single-tuned resonance condition,

$$\omega_0 L = r_0(\omega_0 CR) \quad ,$$ (24)

and expressing R_g in terms of reflection coefficient, Γ_0, Equation 23 may be manipulated into the form

$$\Delta f = \frac{1 + \left(\dfrac{R_s}{r_0}\right)}{\pi RC(1 + \Gamma_0)} \quad .$$ (25)

An inspection of Equation 25 shows that bandwidth becomes inversely proportional to the RF voltage gain of the tunnel diode circuit. Also, the maximum gain-bandwidth product is equal to $(1/\pi RC)$, which is in agreement with derivations contained in the literature (Reference 13) for the single-tuned circuit case.

Figure 7 illustrates a plot of β vs. bandwidth, with values of Δf calculated from Equation 25 for the example diode under conditions of V = -0.07 volts and circuit resonance at 6 Gc. Figure 7 also contains a plot of β vs. bandwidth as measured on the tuned detector mount that was utilized for obtaining the experimental C-band data. This particular detector mount design did not have a bandwidth performance equal to that of a fixed element, single-tuned circuit because of the variation in R_g and L with frequency. Note the characteristic slope of approximately 6 db per octave in β vs. Δf.
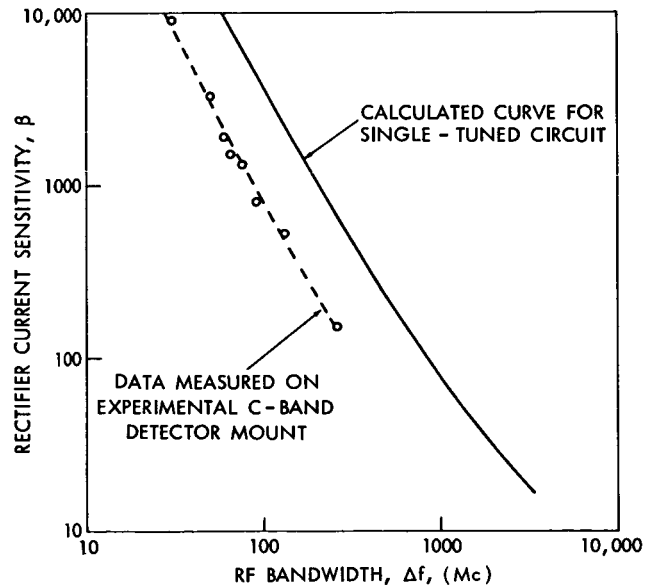
Bandwidth performance is always dependent upon the particular circuits that are utilized in coupling the generator source to the

Figure 7—β vs. RF bandwidth for example diode under conditions V = -0.07 volts and circuit resonance at 6 Gc. The calculated curve assumes that R_g, L, and r_0 are frequency independent.

---

*It is assumed that the reader recognizes the fact that the circuit of Figure 1 is not actually a fixed element, single-tuned circuit because of frequency dependence in R_g, L, and r.

diode. In the extensive literature that exists on the gain-bandwidth products of amplifiers (References 23 to 32), Matthaei (Reference 23) and others have pointed out that considerable bandwidth improvements may be obtained through proper design of more complex impedance transformation circuits between the generator source and the diode.

NOISE OF TUNNEL DIODE AND VIDEO CIRCUIT

From the standpoint of low-level video detection, one of the most important characteristics of the tunnel diode is its low $1/f$ (flicker) noise. Investigators (References 4, 33, and 34) have found that the $1/f$ noise corner frequency is on the order of 1 Kc when the diodes are operated in the low-voltage, positive-conductance region. In fact, for this bias region the tunnel diode (or back diode) has a low-noise performance comparable to the hot carrier (Reference 3) diode. When biased to the peak current point and beyond into the negative resistance region, the $1/f$ noise corner frequency increases steadily (References 22, and 34 to 37) and can deteriorate markedly as the valley region is approached, apparently because of the noisy character of the valley region excess current. Valley region excess video noise varies from one diode to another (Reference 34) but it is generally always high enough that this region of operation should be avoided for high-sensitivity applications. Therefore, the present video noise discussion will proceed on the assumption that the tunnel diode bias voltage excursion shall avoid entering the valley region in order that $1/f$ noise may remain reasonably small.*
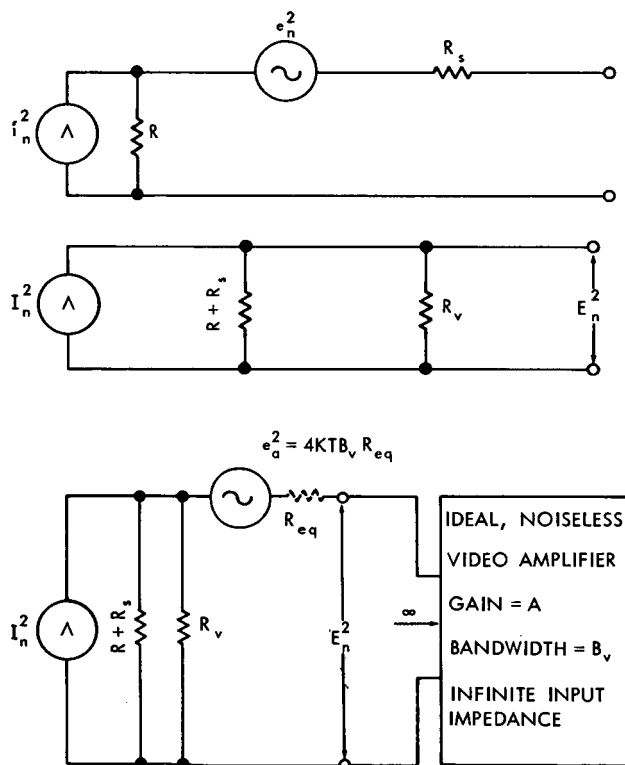
If $1/f$ noise is neglected, then the diode video noise can be attributed to shot noise and thermal noise components which have been shown (References 17, 38 and 39) to be represented by the equivalent circuit of Figure 8(a), where e_n^2 and i_n^2 are given by

$$e_n^2 = 4 K T B_v R_s \quad \text{and} \quad (26)$$

$$i_n^2 = 2 q I_{eq} B_v \ , \quad (27)$$

Figure, 8—Equivalent video noise circuits (midband): (a) Tunnel diode alone, (b) Tunnel diode plus video circuit resistance, R_v, (c) Tunnel diode plus R_v plus excess amplifier noise e_a^2.

*Obviously, if the "video bandwidth" upper frequency limit happens to be in the kilocycle range of frequency, then the $1/f$ noise may not be negligible and its contribution must be accounted for.

12

where

B_v = video noise bandwidth,

$q = 1.6 \cdot 10^{-19}$ coulombs,

I_{eq} = equivalent shot noise current, and

K = Boltzmann's constant.

The equivalent shot noise current, I_{eq}, is related to the actual diode bias current, I, by the derived expression (Reference 17)

$$I_{eq} = I \coth \frac{qV}{2KT} \cdot \qquad (28)$$

A plot of I_{eq} for our example diode is shown in Figure 9, where it will be noted that I_{eq} departs considerably from I near zero bias. At zero bias, I_{eq} must equal the value corresponding to the thermal noise of the conductance, G_0; i.e.,

$$i_{n0}^2 = 4KTG_0 B_v \quad \text{or} \quad I_{eq0} = \frac{2KTG_0}{q} \cdot \qquad (29)$$
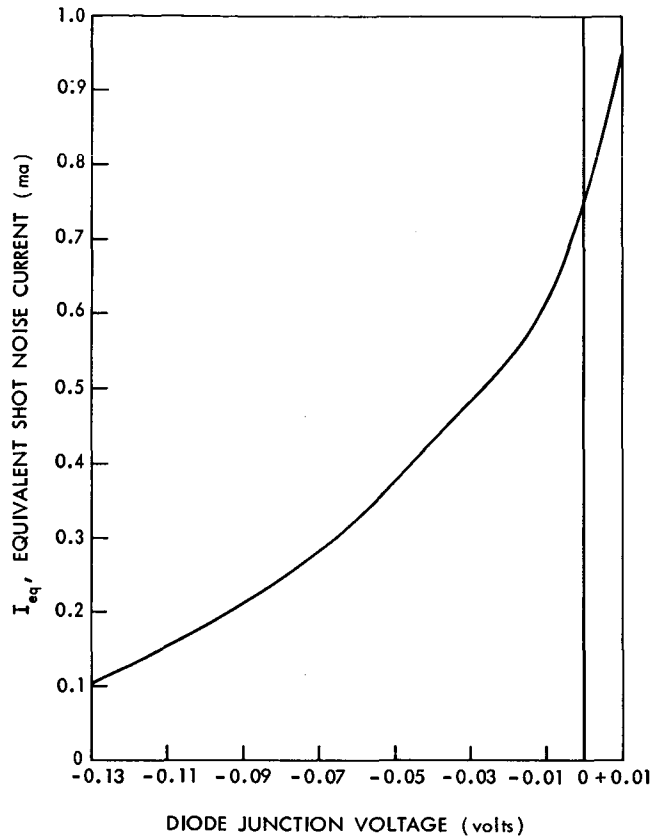

Figure 9—Equivalent shot noise current, I_{eq}, versus junction voltage for example diode.

In addition to the diode noise, a practical video detector is always associated with an equivalent video circuit resistance, R_v, which generates the thermal noise voltage $4KTB_v R_v$. The resistance R_v includes the bias circuit for the diode plus the input impedance of the amplifier utilized with the detector. Figure 8(b) illustrates the midband* equivalent video noise circuit, where R_v noise plus diode noise contributions have been lumped into the equivalent noise current generator, I_n^2. I_n^2 will be equal to

$$I_n^2 = \frac{2q\, I_{eq}\, B_v}{(1 + GR_s)^2} + \frac{4KTB_v\, R_s}{(R + R_s)^2} + \frac{4KTB_v}{R_v} \cdot \qquad (30)$$

The output noise voltage, E_n^2, produced by I_n^2 is therefore

$$E_n^2 = I_n^2 R_i^2 \quad , \qquad (31)$$

---

*"Midband" refers to the middle of the video passband determined by the video amplifier.

where

$$R_i = \left(\frac{R_v(R_s + R)}{R_v + R_s + R}\right) . \tag{32}$$

R_i is the total equivalent resistance, being the parallel combination of R_v and $(R_s + R)$. It should be pointed out that Equation 32 is particularly significant for a tunnel diode detector because of the fact that R can become large and may also be negative. Either condition will restrict the maximum value that R_v can take. For instance, the stability criteria for the video circuit requires that R_i be positive, so that from Equation 32 one obtains the necessary condition that

$$R_v < |R_s + R| \quad \text{for negative R}. \tag{33}$$

Furthermore, it may be necessary to place an upper bound upon R_i in order to obtain sufficient video bandwidth, and this upper bound on R_i will, in turn, restrict the maximum value that R_v may have.

Amplifier excess noise, which is always present in high-sensitivity video detection, can be represented by placing an equivalent noise generating resistance (References 1, and 40) R_{eq}, between the detector video circuit and an ideal amplifier with an infinite input impedance as shown in Figure 8(c). The total noise voltage, E_n^2, therefore has e_a^2 added to Equation 31, becoming

$$E_n^2 = I_n^2 R_i^2 + 4KTB_v R_{eq} . \tag{34}$$

Values of R_{eq} are readily determined from measurements of the amplifier gain, bandwidth, and r.m.s. output noise under known input circuit conditions.

Video noise bandwidth has never been satisfactorily standardized and is usually different for each detector application, so that it is desirable to normalize all noise contributions in terms of noise per cycle of video bandwidth. Thus, dividing Equation 34 and Equation 30 by B_v we obtain,

$$\left(\frac{E_n^2}{B_v}\right) = \left(\frac{I_n^2}{B_v}\right) R_i^2 + 4KTR_{eq} \tag{35}$$

and

$$\left(\frac{I_n^2}{B_v}\right) = \frac{2q I_{eq}}{(1 + GR_s)^2} + 4KT\left[\frac{1}{R_v} + \frac{R_s}{(R + R_s)^2}\right] . \tag{36}$$

A plot of $\sqrt{I_n^2/B_v}$ versus diode junction voltage for our example diode is shown in Figure 10 under two R_v conditions: (a) R_v held constant at 265 ohms for all bias voltages; (b) Maximum R_v for each
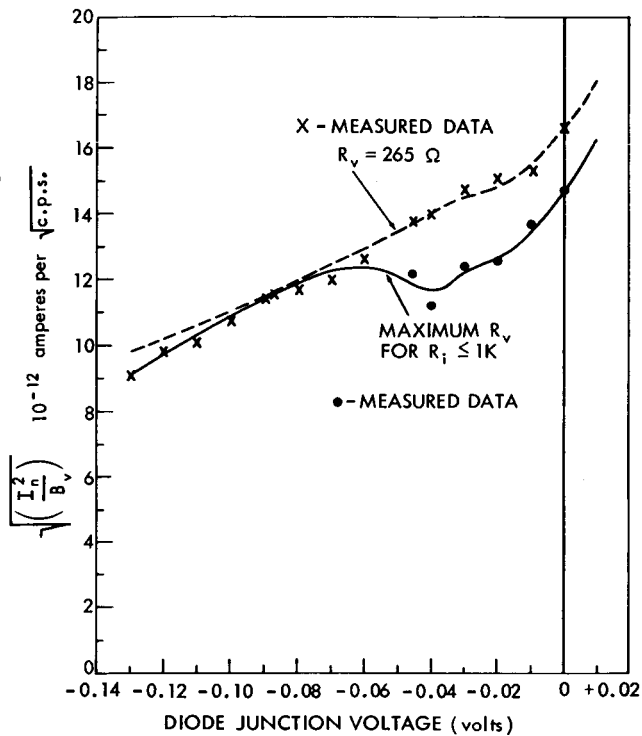
14

Figure 10—$\sqrt{I_n^2/B_v}$ versus junction voltage for example diode under two R_v conditions.
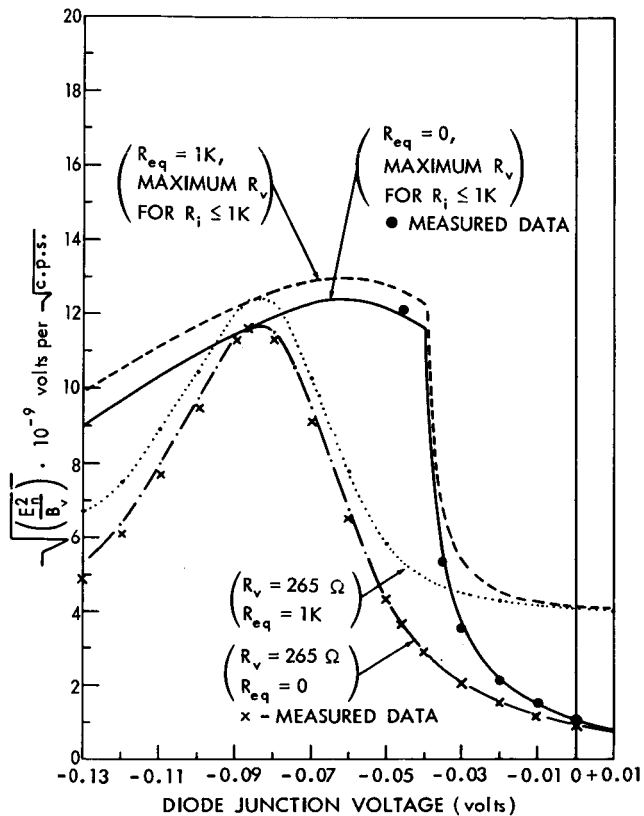

Figure 11—$\sqrt{E_n^2/B_v}$ versus junction voltage for example diode under two R_v conditions for $R_{eq} = 0$ and $R_{eq} = 1K$.

bias voltage subject to the restriction that R_i $\leq$ 1000 ohms. The 1K upper bound chosen for R_i represents a typical design value for wideband video detector circuits, and the two R_v conditions encompass the resultant design range for R_v. For diode junction voltage above -0.04 volts, R_v can be infinite so that this segment of the lower curve (maximum R_v) in Figure 10 represents the noise current contributed by the diode alone. The measured data points shown in Figure 10 were obtained from r.m.s. noise voltage measurements* on the example diode, and they agree with the calculated curves within the limits of experimental measurement error.

Figure 11 illustrates the total r.m.s. noise voltage per $\sqrt{c.p.s.}$, $\sqrt{E_n^2/B_v}$, versus diode junction voltage for the same conditions utilized in Figure 10 plus the addition of amplifier excess noise. The set of curves for $R_{eq} = 0$ give the noise voltage that could be obtained with an ideal noiseless amplifier, and the set of curves for $R_{eq} = 1K$ illustrates the noise voltage that would be obtained with a typical transistor video amplifier of recent design. Note that the experimental measured data points* on the example diode are in very close agreement with the calculated curves.

---

*The video amplifier utilized in conducting the noise measurements on the example diode had the following characteristics: Gain — 10,000; Bandwidth — 2 mc.; Input Impedance — 50 K and 60 pf; Noise R_{eq} — 730 ohms. Noise due to R_{eq} was subtracted out in order to obtain diode noise data.

These noise curves point up several interesting features associated with tunnel diode video detectors:

(a) The considerable variation in noise voltage level versus diode bias reflects the variation that occurs in R_i (Equation 32). Video resistance R_v affects the shape and peak value of the R_i variation.

(b) In the vicinity of zero bias where R_i becomes less than 100 ohms, amplifier noise can easily dominate the diode noise and thus degrade sensitivity.

(c) When the diode is biased near its peak current point or beyond into the negative resistance region, R_i increases such that the diode noise becomes dominant over the amplifier noise. This latter situation is very desirable for practical high-sensitivity detection.

TANGENTIAL SENSITIVITY

Tangential sensitivity (References 41 and 42) is defined as that signal level which raises the noise by its own width on an oscilloscope pulse-plus-noise presentation. This sensitivity criterion has the disadvantage of being somewhat dependent upon particular receiver conditions and particular observer interpretation, but it is still the most practical criterion available for measuring the sensitivity performance of low-level video detectors. It is generally found to be consistent within ±1 db in RF power level for given receiver conditions and a given observer. To overcome the problem of changing receiver conditions and/or changing observers, it is necessary to measure the average signal-to-noise ratio actually associated with a given receiver-observer set-up, and then correct the measured data to the fixed reference value of 8 db which is utilized in the literature for calculation and comparison of tangential sensitivity performance. 8 db results in a voltage ratio of 2.5 in the video circuit, and this value will be employed in the calculations to follow.

The minimum video detector equivalent circuit* needed for computing tangential sensitivity is shown in Figure 12. It consists of the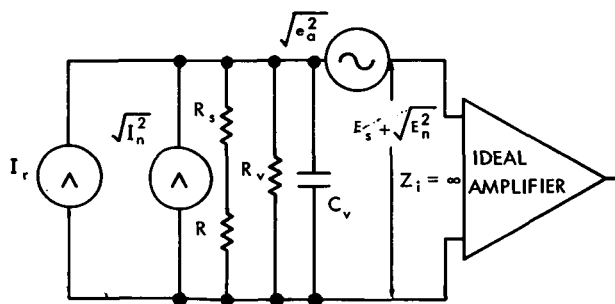 midband video equivalent noise circuit discussed in the preceeding section, plus the rectification current generator, I_r, and the total shunt capacitance, C_v. Shunt capacitance includes the amplifier input capacitance, the detector RF bypass condenser, and the shielded cable capacitance, if present. The presence of C_v places an upper bound on the values that R_i may have because of bandwidth considerations. The bandwidth of the circuit must be adequate for the pulse response required and, in addition, it is always desirable to have the input circuit bandwidth

Figure 12—Minimum video equivalent circuit.

*The terminology "minimum circuit" is used in the sense that there can never be fewer components than shown in Figure 12. Needless to say, actual detector video circuits are oftentimes considerably more complicated due to the presence of chokes, transformers, pulse peaking circuits, etc.

exceed the amplifier bandwidth in order to minimize amplifier noise contribution. The 3 db bandwidth point will occur when $\omega R_i C_v = 1$, so that we require

$$R_i < \frac{1}{2\pi C_v B_v} \cdot \tag{37}$$

This upper bound on R_i may also be expressed in terms of τ, the pulse rise time between 10 and 90 percent amplitude points, since video bandwidth and pulse rise time have the approximate product (Reference 43)

$$\tau B_v \approx 0.35 , \tag{38}$$

so that

$$R_i < \frac{\tau}{2.2 C_v} \cdot \tag{39}$$

This restriction upon R_i results in a restriction upon the maximum value of R_v via Equation 32; i.e., from (32) we obtain

$$R_v \simeq \left[\frac{R_i}{1 - \dfrac{R_i}{R_s + R}} \right] . \tag{40}$$

Assuming that R_i is adjusted for adequate safety margin in Equation 37, the voltage E_s developed is simply

$$E_s = I_r R_i = \beta P_i R_i , \tag{41}$$

where βP_i was substituted for the rectification current from Equation 6. The tangential sensitivity ratio defines a particular input RF power level, $P_i = P_t$, such that the 8 db ratio of E_s to $\sqrt{E_n^2}$ is obtained,

$$\frac{E_s}{\sqrt{E_n^2}} = 2.5 = \frac{\beta R_i P_t}{\sqrt{B_v} \cdot \sqrt{\left(\dfrac{I_n^2}{B_v}\right) R_i^2 + 4KTR_{eq}}} \tag{42}$$

or

$$P_t = \left(\frac{2.5 \sqrt{B_v}}{\beta}\right) \bigg/ \sqrt{\left(\frac{I_n^2}{B_v}\right) + \left(\frac{4KTR_{eq}}{R_i^2}\right)} \cdot \tag{43}$$

17

Note that when the amplifier noise contribution becomes negligible, Equation 43 simplifies to

$$P_t = 2.5 \cdot \frac{I_n}{\beta}$$

(44)

Equation 44 can be plotted vs. frequency for our example diode by utilizing values of β from Figure 5 and values of $\sqrt{I_n^2/B_v}$ from Figure 10. The resultant tangential sensitivities are shown plotted in Figure 13. The left hand scale gives $P_t/\sqrt{B_v}$ in dbm per $\sqrt{c.p.s.}$, and the right hand scale gives P_t in dbm for a video noise bandwidth of 1 mc. The comments which were made on the β curves of Figure 5 would apply equally well to Figure 13, since there is only a small relative shift in the curves caused by the change in noise-current with bias voltage. In addition, it will be noted that the tangential sensitivities that can be achieved at frequencies below f_r are at least an order of magnitude better than the performance of other types of diodes (References 1 to 3).

The calculated curves of Figure 13 have been experimentally verified with the example diode at frequencies of 3, 5, 6, and 7 Gc, as illustrated by the data points plotted.

The experimental receiver set-up for measuring tangential sensitivity had a consistent value of 4 for the ratio of observer interpreted peak-to-peak noise amplitude on the oscilloscope as compared to the measured r.m.s. value. This results in a tangential sensitivity signal to noise ratio of 12 db on the video side for the experimental measurements. Since the calculated curves are based upon the fixed reference value of 8 db, all experimental data was corrected by the square root of the difference, or 2 db, in order to obtain a valid comparison with the calculated curves. (The square root of the 4 db difference must be taken because low-level detection is square-law and the video difference must be referred to the RF side of the detector.)
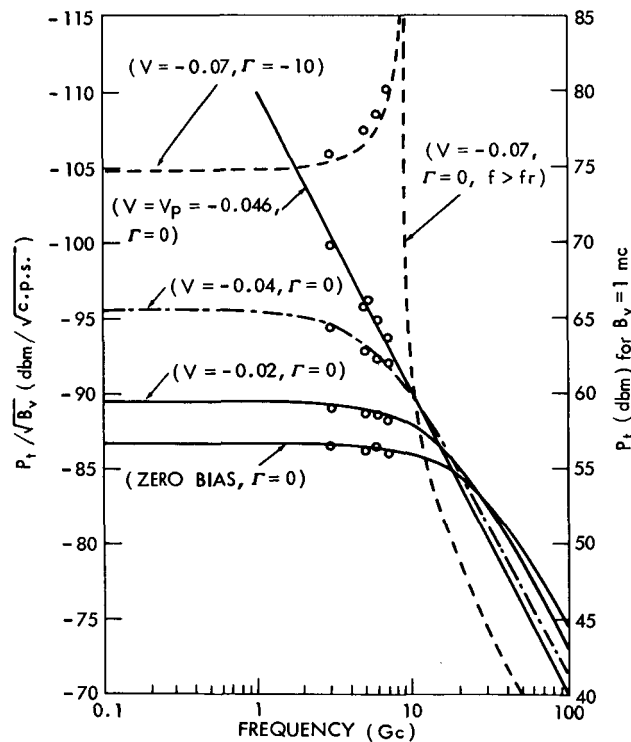
A typical variation in tangential sensitivity vs. bias for the example diode is shown in Figure 14, calculated by utilizing values of β from Figure 6(a) and values of $\sqrt{E_n^2/B_v}$ from Figure 11 with maximum R_v for $R_i \leq 1K$ and amplifier noise R_{eq} either zero or 1K as denoted on the curves. It will be noted that amplifier noise reduces tangential sensitivity significantly in the vicinity of zero bias, but becomes negligible when the diode is biased near the peak current point or beyond. Sensitivity drops to zero very sharply at the inflection point where β goes through zero (Figure 6(a)). The highest peak tangential sensitivity point is readily

Figure 13—Tangential sensitivity versus frequency for example diode under conditions of $R_i \leq 1K$ and $R_{eq} = 0$.

determined via bias adjustment and is usually chosen as the detector operating bias point. This operating point will shift slightly as a function of Γ and/or frequency, shifting closer to the inflection point for increasing values of Γ and/or frequency.

A typical variation in tangential sensitivity vs. RF bandwidth for the example diode is shown in Figure 15. These were calculated by utilizing values of β and Δf from Figure 7 which were determined on the assumption of fixed element, single-tuned circuit behavior. The associated noise current was obtained from Figure 10 for an operating bias point of -0.07 volts. Figure 15 also contains a plot of P_t vs. Δf as measured on the example diode in a tuned C-band detector mount. This particular mount did not have a bandwidth performance equal to that of a fixed element, single-tuned circuit because of the frequency dependence of R_g and L. Since the tangential sensitivity variations mainly reflect the variations that occur in β, the bandwidth comments in the previous section apply directly here.

An example of the increased bandwidth that can be obtained from a more complex circuit design is shown in Figure 16 where the performance of a double-tuned response design is compared with a single-tuned response design. In this particular instance the bandwidth was improved by a factor of three.

As a practical note, it should be pointed out that a P_t vs. Δf plot provides a very effective means for evaluating the relative performance of tunnel diodes when measured in the same detector mount at the same resonant frequency.

FIGURE OF MERIT, COMPARISON WITH HOT CARRIER DIODE

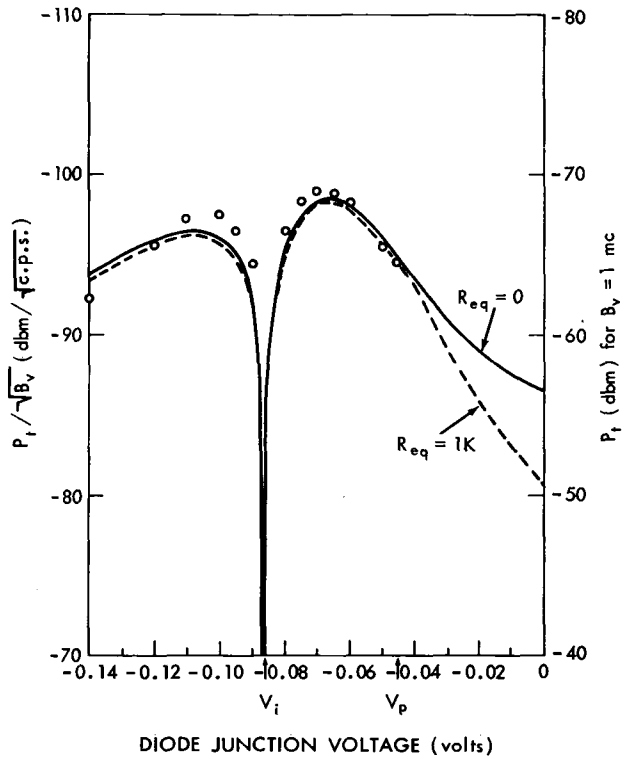The figure of merit, M, which is often utilized as a criterion of excellence for video

Figure 14—Tangential sensitivity vs. junction voltage for example diode under conditions of $R_i \leq 1K$ and R_{eq} either zero or 1K.
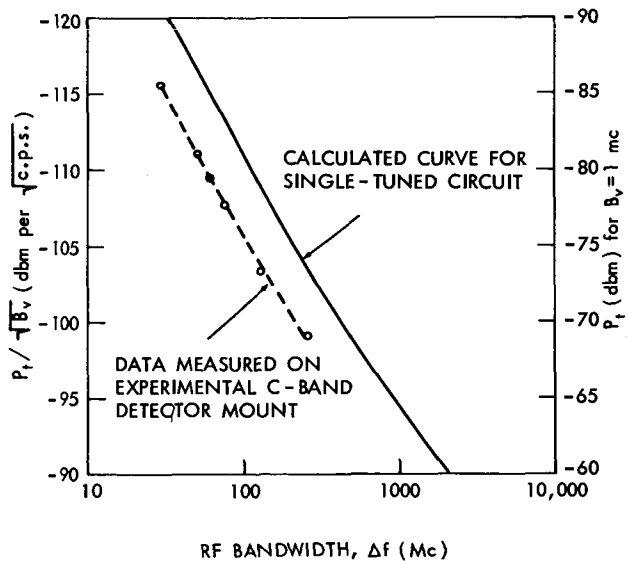
Figure 15—Tangential sensitivity vs. RF bandwidth for example diode under conditions of V = -0.07 volts and circuit resonance at 6 Gc.
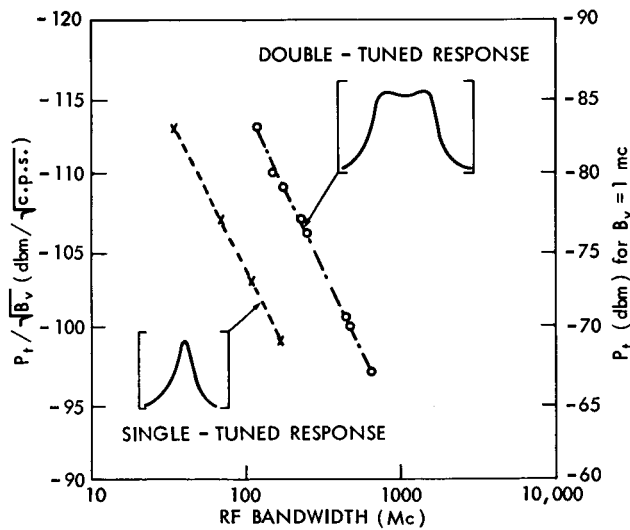
19

Figure 16—Experimental comparison between single-tuned response and double-tuned response. MS-1202 diode at 6 Gc.
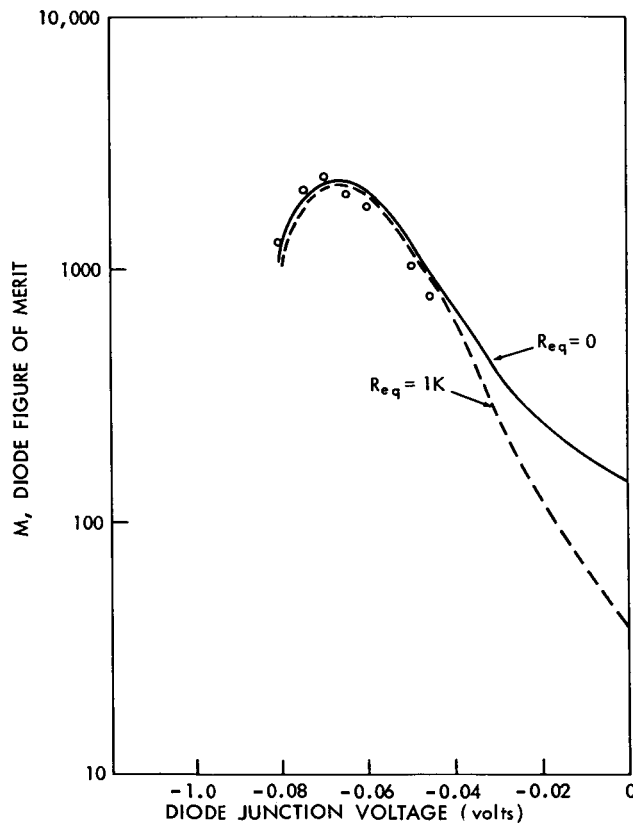

Figure 17—Figure of merit, M, vs. junction voltage for example diode under conditions of R_g = 85 ohms, and detector circuit resonance at 3 Gc.

detectors, is defined as (Reference 1)

$$M = \frac{\sqrt{4KTB_V}}{P_i} \cdot \frac{E_s}{\sqrt{E_n^2}} \cdot \quad (45)$$

Substituting Equations 41 for E_s and 34 for E_n^2, one obtains,

$$M = \frac{\beta}{\sqrt{\frac{I_n^2}{4KTB_V} + \left(\frac{R_{eq}}{R_i^2}\right)}} \cdot \quad (46)$$

Utilizing values of β from Figure 6(a) and noise current from Figure 10, substitution into Equation 46 results in a typical figure of merit plot vs. junction voltage shown in Figure 17 for amplifier noise R_{eq} of zero and 1K. It is important to note that when the diode is biased into the negative resistance region, amplifier noise is no longer significant and figures of merit in the thousands are readily achieved.

The figure of merit criterion offers the best means for comparing the relative sensitivity performance of a tunnel diode against a hot carrier diode. For the purposes of this comparison, it is reasonable to neglect amplifier noise, i.e., let $R_{eq} = 0$, so that Equation 46 simplifies to

$$M = \frac{\beta}{\sqrt{\frac{I_n^2}{4KTB_V}}} \cdot \quad (47)$$

For the tunnel diode, values of β are calculated from Equations 16, 18, or 19 depending upon whether G is positive, zero, or negative; and the noise current is calculated from Equation 30.

For the hot carrier diode, values of β are calculated only from Equation 16 since G is

20

always positive; and the noise current may be approximated by the thermal conductance noise (Reference 3), since this is a unique low-noise property of the diode if the video bandwidth lies above the flicker noise corner frequency.

$$\text{(hot carrier diode)} \quad I_n^2 \approx \frac{4\,K\,T\,B_V}{R_s + R} \quad \cdot \tag{48}$$

Upon substituting Equations 16 and 48 into 47 and assuming optimum performance ($\Gamma = 0$), the figure of merit for a hot carrier diode, denoted as M_{hc}, becomes

$$M_{hc} = \frac{\beta_0 \sqrt{R_s + R}}{\left[1 + \left(\frac{f}{f_c}\right)^2\right]} \quad \cdot \tag{49}$$

β_0 is particularly simple for a hot carrier diode because the ratio of G and its first derivative remains constant, i.e., the diode current may be written as (Reference 2)

$$I = I_s \left(e^{\alpha V} - 1\right) \;, \tag{50}$$

where

$$\alpha = \frac{qV}{nKT} \approx 38 \;,$$

I_s = saturation current, and

V = diode junction voltage.

Then

$$G = \frac{dI}{dV} = \alpha\, I_s\, e^{\alpha V} \;, \text{and} \tag{51}$$

$$G' = \frac{dG}{dV} = \alpha^2\, I_s\, e^{\alpha V} \;. \tag{52}$$

Thus, the ratio of G' to G is equal to α and substitution into Equation 15 results in

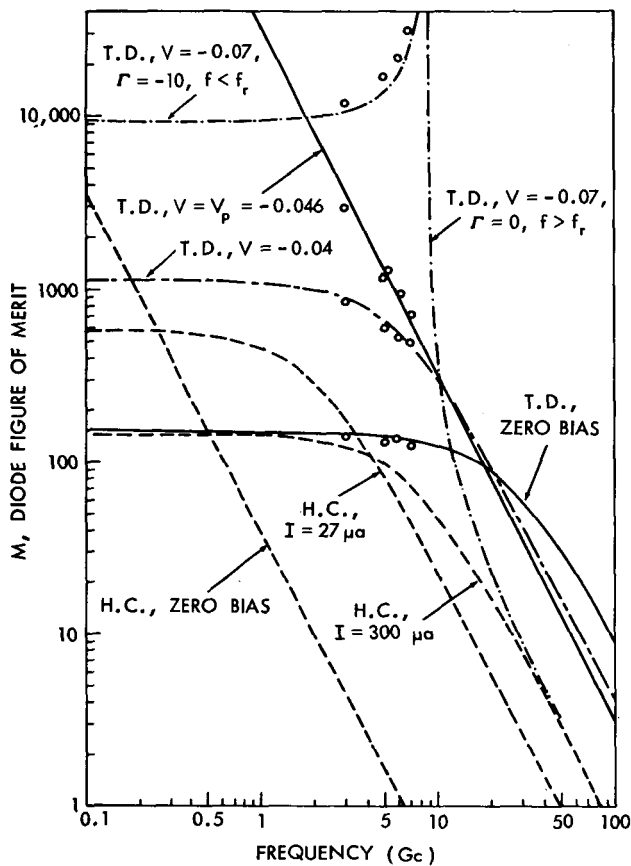$$\text{(hot carrier diode)} \quad \beta_0 = \frac{\alpha}{2(1 + GR_s)^2} \approx \frac{19}{(1 + GR_s)^2} \quad \cdot \tag{53}$$

Figure 18—Figure of merit, M, vs. frequency for example diode and a hot carrier diode, hpa-2350, under various bias conditions.

Upon substituting this β_0 into (49) and simplifying, M_{hc} becomes

$$M_{hc} \approx \frac{19\sqrt{R}}{(1 + GR_s)^{3/2}\left[1 + \left(\frac{f}{f_c}\right)^2\right]} = \frac{M_{hco}}{\left[1 + \left(\frac{f}{f_c}\right)^2\right]} \quad (54)$$

where f_c is given by Equation 17.

For calculation, the published characteristics of typical hpa-2350 diodes (Reference 3) were utilized: series resistance $R_s \approx 12$ ohms, junction capacitance $C \approx 0.75$ pf, and $I_s = 8 \cdot 10^{-9}$ amperes. The figure of merit performance for this particular hot carrier diode is illustrated by the dashed-line curves in Figure 18 for three bias conditions: zero bias, $I = 27\mu$ amps, and $I = 300\mu$ amps. These calculated curves are found to be in close agreement with the published tangential sensitivity data for the diode (Reference 3) when cross-checked via the relationship derived from Equation 45,

$$\left(\frac{\sqrt{B_v}}{P_t}\right) = \frac{M}{2.5\sqrt{4KT}} = 3.16 \cdot 10^9 M \quad (55)$$

The curves clearly illustrate the trade off between M_{hco} and f_c as the bias current, I, is increased.

The example diode was utilized for calculating the tunnel diode performance as illustrated by the lines labelled "T.D." in Figure 18 for four junction voltage conditions; zero bias, $V = -0.04$ volts, $V = V_p$, and $V = -0.07$ volts. Some experimental confirmation data points are included. It is noteworthy that the tunnel diode has a better sensitivity capability than the hot carrier diode for the examples shown here, even when the tunnel diode is restricted to positive conductance biasing. When biased to V_p or beyond into the negative resistance region, as illustrated by the broken-line curve for $V = -0.07$ volts, the tunnel diode is capable of at least an order of magnitude improvement in sensitivity over the hot carrier diode for frequencies below f_r.

The reader is cautioned against over-generalization of the relative diode sensitivity performance shown in Figure 18, because it is noteworthy that the curves are based upon only two particular diode examples and, also, the 1/f noise was assumed to be negligible for both diodes. When biased in its negative resistance region, a tunnel diode will have a much higher 1/f noise corner

frequency than the hot carrier diode, and this factor can become important for video bandwidths below 1 megacycle.

CONCLUSIONS

A low-level detection analysis of the tunnel diode has been presented with the aim of covering its detection behavior for any bias condition, particularly in the negative resistance region. It has been shown that for negative resistance biasing, the tunnel diode exhibits the following interesting detection properties:

(a) For a bias excursion through the inflection point, the detector shows a discriminator-like, rectification reversal behavior, with the zero output point anchored precisely at the inflection bias point.

(b) For frequencies below resistive cut-off, sensitivity is proportional to $(1 - \Gamma^2)$, where Γ^2 is the RF power gain of the detector viewed as a reflection-type amplifier, so that unusually high sensitivities can be achieved.

(c) For frequencies above resistive cut-off, the sensitivity drops rather abruptly and quickly becomes inferior to the zero bias sensitivity.

The unusually high sensitivities which are made possible via control of Γ^2 must necessarily be subject to all of the trade offs that are associated with high-gain RF amplifiers, and it was shown that the usual gain-bandwidth product applies directly, i.e., a higher sensitivity can only be achieved at the expense of a smaller bandwidth. Other trade offs, familiar to the tunnel diode amplifier art, include greater temperature variation, more critical bias regulation, a lower saturation power level, and more critical circuit stability conditions. If one is willing to accept the trade offs, then sensitivities an order of magnitude better than any other video detector are readily achieved. In fact, the sensitivity can actually be pushed to the point of being competitive with a superheterodyne receiver under certain conditions.

A practical by-product of this detection study was the observation that the rectified current from a tunnel diode amplifier provides a very sensitive and valuable tool during the design and adjustment phase of an amplifier since it can be utilized to monitor bias stability, spurious oscillation, bandpass shape, bandwidth adjustment, temperature effects, saturation effects, extraneous signals, etc. The rectified current could also be incorporated into a feedback loop for bias point control or automatic gain control.

Special mention must be made of the peak current bias point of a tunnel diode. It was shown that this particular bias point results in a sensitivity inversely proportional to the square of the frequency, and this behavior results in unusually high sensitivities at the lower microwave frequencies. The easy stability conditions involved in peak current biasing make it a very attractive operation point.

REFERENCES

1. Torrey, H. C., and Whitmer, C. A., "Crystal Rectifiers," *Mass. Inst. Tech. Rad. Lab. Series,* vol. 15: Chapter 11; New York: McGraw-Hill, 1948.

2. Hall, R. N., "Design of the Hot Carrier Mixer and Detector," *IEEE International Solid-State Circuits Conference Digest,* VIII: 98-99, February 1965.

3. Sorensen, H. O., "Using the Hot Carrier Diode as a Detector," *Hewlett-Packard Journal,* 17: 4, December 1965.

4. Eng, S. T., "Low-noise Properties of Microwave Backward Diodes," *IRE Trans.* MTT-9:419-42; Sept. 1961.

5. Montgomery, M. D., "The Tunnel Diode as a Highly Sensitive Microwave Detector," *Proc. IRE* 49:826-827, 1961.

6. Reindel, J., "The Tunnel Diode as a C. W. Detector, *Proc. IEEE* 51:1677-1678, 1963

7. Chase, P. E., and Chang, K. K. N., "Tunnel Diodes as Millimeter Wave Detectors and Mixers," *IEEE Trans.* MTT-11:560-561, 1963.

8. Gabriel, W. F., "The Versatile Tunnel-Diode Video Detector," *IEEE International PTGMTT Symposium Digest,* pp. 157-162, May 1964.

9. Wright, R. O., and Goldman, R. L., "Aluminum Alloy Junction Backward Diodes in Microwave Detection Systems," *IEEE International Solid State Circuits Conference Digest,* VIII: 100-101, February 1965.

10. Mouw, R. B., and Schumacher, F. M., "Tunnel Diode Detectors," *Microwave J.* 9:27-36, January 1966.

11. Van Voorhis, S. N., ed., "Microwave Receivers," *Mass. Inst. Tech. Rad. Lab. Series,* vol. 23: Chapter 19; New York: McGraw-Hill, 1948.

12. Klipper, H., "Sensitivity of Crystal Video Receivers with R. F. Pre-Amplification, " *Microwave J.* 8:85-92, Aug. 1965.

13. Hines, M. E., "High-frequency Negative Resistance Circuit Principles for Esaki Diode Applications," *Bell Syst. Tech. J.* 39:447-513, 1960.

14. Gentile, S. P., "Basic Theory and Application of Tunnel Diodes," Princeton, N. J.: Van Nostrand, 1962.

15. Nergaard, L. S., and Glicksman, M., eds. "Microwave Solid-State Engineering," Princeton, N. J.: Van Nostrand, 1964.

16. Chang, K. K. N., "Parametric and Tunnel Diodes," Englewood Cliffs, N. J.: Prentice-Hall, 1964.

17. Chow, W. F., "Principles of Tunnel Diode Circuits," New York: Wiley, 1964.

18. Smilen, L. I., and Youla, D. C., "Stability Criteria for Tunnel Diodes Shunted by Resistance and Capacitance," *Proc. IEEE* 51:1233, 1963.

19. Davidson, L. A., "Optimum Stability Criterion for Tunnel Diodes Shunted by Resistance and Capacitance," *Proc. IEEE (Correspondence):* 51: 1233, September 1963.

20. Frisch, I. T., "A Stability Criterion for Tunnel Diodes," *Proc. IEEE* 52:922-923, 1964.

21. Bandler, J. W., "Stability and Gain-Prediction of Microwave Tunnel-Diode Reflection Amplifiers," *IEEE Trans.* MTT-13:814-819, 1965.

22. Lowry, H. R., et al., "Tunnel Diode Manual," 1st Edition, New York General Electric, 1961.

23. Matthaei, G. L., "A Study of the Optimum Design of Wide-Band Parametric Amplifiers and Up-Converters," IRE Trans. MTT-7:23-38, January 1961.

24. Seidel, H., and Herrmann, G. F., "Circuit Aspects of Parametric Amplifiers," *IRE Wescon Conv. Rec.* 3: Pt. 2-Circuit Theory, 83-90, 1959.

25. Gilden, M., and Matthaei, G. L., "Practical Design and Performance of Nearly Optimum Wideband Degenerate Parametric Amplifiers," IRE Trans. MTT-9:484-490, November 1961.

26. Lepoff, J. H., and Wheeler, G. J., "Octave Bandwidth Tunnel-Diode Amplifiers," IEEE Trans. MTT-12: 21-23, January 1964.

27. Scanlon, J. O., and Lim, J. T., "Effect of Parasitic Elements on Reflection Type Tunnel Diode Amplifier Performance," IEEE Trans. MTT-13: 827-836, November 1965.

28. Getsinger, W. J., "Prototype for Use in Broadbanding Reflection Amplifiers," IEEE Trans. MTT-11: 486-497, November 1963.

29. Aron, R., and Sard, E. W., "Gain Bandwidth Relations in Negative-Resistance Amplifiers," *Proc. IRE* 49:355-356, 1961.

30. Hamasaki, J., "Low-Noise and Wide-Band Esaki Diode Amplifier with Comparatively High Negative Conductance Diode at 1.3 Gc/s," IEEE Trans., MTT-13: 213-223, 1965.

31. Sard, E. W., "Tunnel (Esaki) Diode Amplifiers with Unusually Large Bandwidths," *Proc. IRE* 48:357-358, 1960.

32. Logan, J. S., "Gain vs. Bandwidth Limits for Esaki Diode Amplifiers," *Proc IRE* 49:832, 1961.

33. Follmer, W. C. "Low Frequency Noise in Backward Diodes," *Proc. IRE* 49:1939-1940, 1961.

34. Agouridis, D. C. and Van Vliet, K. M., "Noise Measurements on Tunnel Diodes," *Proc. IRE* 50:2121, 1962.

35. Montgomery, M. D., "Excess Noise in Germanium and Gallium-Arsenide Esaki Diodes in Negative Resistance Region," *J. Appl. Phys.* 32: 2408-2410, November 1961.

36. Burkhard, M. D., "Tunnel Diode Audio-Frequency Noise," *Proc. IRE* 50:2487-2488, 1962.

37. Giblin, R. A., "Noise-Spectrum Measurements on Tunnel Diodes in the Frequency Range 5KC to 10MC," *Electronic Eng.* 766-769, 1964.

38. Tiemann, J. J., "Shot Noise in Tunnel Diode Amplifiers," *Proc. IRE* 48:1418-1423, 1960.

39. Pucel, R. A., "The Equivalent Noise Current of Esaki Diodesk" *Proc. IRE* 49: 1080-1081, 1961.

40. Rheinfelder, William A., "Design of Low Noise Transistor Input Circuits," New York: Hayden Book, 1964.

41. Montgomery, Carol Gray, "Technique of Microwave Meaurements," Mass. Inst. Tech. Rad. Lab. Series, vol. 11: 228-229; New York: McGraw-Hill, 1947.

42. Van Voorhis, S. N., "Microwave Receivers," Mass. Inst. Tech. Rad. Lab. Series, vol. 23:292, 456, 505; New York: McGraw-Hill, 1948.

43. Valley, G. E., "Vacuum Tube Amplifiers," Mass. Inst. Tech. Rad. Lab. Series, vol. 18: Chapter 2; New York: McGraw-Hill, 1948.

Appendix A

Derivation of β

The rectification current sensitivity, β, is given by the ratio of I_r to P_i,

$$\beta = \frac{I_r}{P_i} \tag{A1}$$

where I_r is the rectified current and P_i is the RF power incident upon the detector. The evaluation of I_r presents a formidable, if not impossible, non-linear circuit analysis task if P_i is not restricted to low levels. However, by restricting P_i to low levels such that the RF voltage excursion on the non-linear diode characteristic is small compared to the radius of curvature, then Taylor series approximations (Reference 1) can be employed to derive an accurate expression for low level rectification.

Figure A1 illustrates a model of a simple tuned microwave detector with dc return, where C_b represents the RF by-pass condenser, R_v is the video circuit resistance, S_1 and S_2 are lengths of RF transmission line of characteristic impedances Z_{01} and Z_{02} respectively; Z_g represents the connected generator source impedance, and V_b is the applied dc bias voltage across the diode. A detailed equivalent circuit representation of this detector is shown in Figure A2 where the diode equivalent circuit (References 1 and 17) elements are defined as follows:

R - differential junction resistance of diode

C - junction capacitance of diode
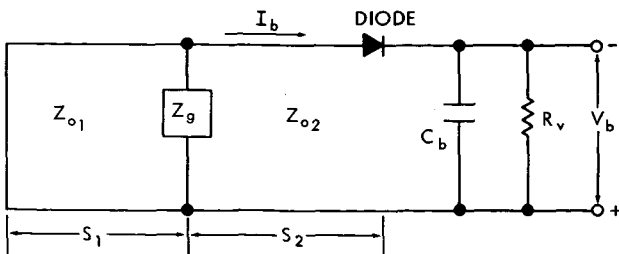
R_s - series resistance of diode

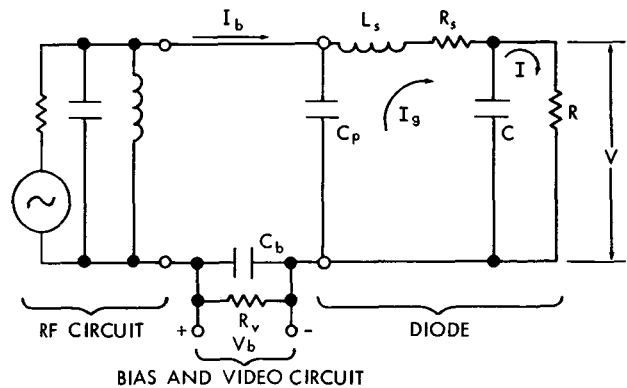Figure A1—Model of a simple tuned microwave detector with dc return.

Figure A2—An equivalent circuit representation of the detector shown in Figure A1.

27

L_s - series inductance of diode

C_p - diode package capacitance plus mounting capacitance

V - voltage across diode junction

I - current through R, including I_b

I_b - dc bias current associated with V_b .

The reader is reminded that the non-linearity of a diode (References 1 and 17) occurs in the V-I characteristic of the junction, and that R in Figure A2 is not the static ratio of V to I but is the differential ratio, (dV/dI), at a particular bias point on the V-I curve.

To convert Figure A2 into a simple equivalent RF circuit, it is convenient to represent the bias voltage across C_b and R_v with an equivalent bias battery, V_b, of zero impedance (the reactance of C_b is very small at microwave frequencies of interest). Then, by utilizing the equivalent series impedance elements seen from the diode junction, one can construct the simple equivalent RF circuit shown in Figure A3. Needless to say, circuit elements R_g and L are frequency dependent.
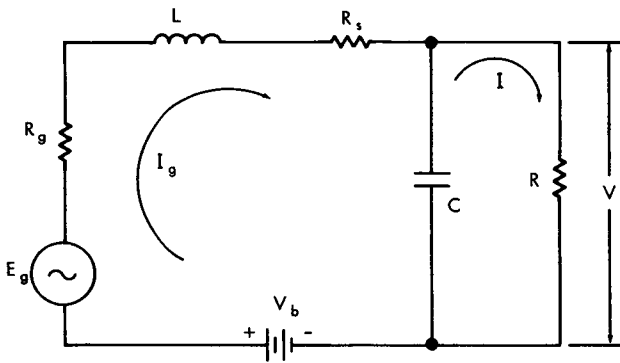

Figure A3—Equivalent RF circuit of detector referred to diode junction.

The non-linear V-I characteristic of the diode junction causes a non-linear relationship between the current I_g and the applied voltages $(V_b + E_g)$. If we assume that E_g is a very small sinusoidal signal,

$$E_g = be^{j\omega t}, \quad b <<< 1 \tag{A2}$$

Then I_g can be conveniently approximated by a Taylor series expansion (Reference 1) of three terms about the bias voltage point V_b,

$$I_g = \phi(V_b + E_g) \approx \phi(V_b) + \phi'(V_b) \cdot E_g + \frac{1}{2} \phi''(V_b) \cdot E_g^2 + \cdots \tag{A3}$$

The first term is the dc bias current, I_b. The second term is the linear RF current component,

$$\phi'(V_b) \cdot E_g = \frac{E_g}{Z} , \tag{A4}$$

where Z is the total series impedance of the circuit at the bias point, i.e.,

$$Z = \left[R_g + R_s + \left(\frac{R}{1 + (\omega CR)^2} \right) \right] + j \left[\omega L - \left(\frac{\omega CR^2}{1 + (\omega CR)^2} \right) \right] . \tag{A5}$$

The third term may be evaluated by squaring the real part of E_g, whereupon

$$\frac{1}{2}\phi''(V_b) \cdot b^2 \cos^2 \omega t = \frac{1}{4}\phi''(V_b) \cdot b^2 \cdot (1 + \cos 2\omega t) \ . \tag{A6}$$

This consists of the rectified current plus a second harmonic component. The second harmonic component is of no interest here, so that Equation A3 may be written,

$$I_g \approx I_b + \frac{E_g}{Z} + I_r \ . \tag{A7}$$

Utilizing this approximation for I_g, it follows that the voltage, V, across the diode junction is given by

$$V \approx V_b - R_s(I_b + I_r) + \frac{Z_j}{Z} \cdot E_g \ , \tag{A8}$$

where Z_j is the equivalent series impedance of the diode junction,

$$Z_j = \left(\frac{1}{G + j\,\omega C}\right) \ . \tag{A9}$$

Note that R_g does not enter into the dc voltage drop in (A8) because R_g is zero at dc. If we define $V_{jb} = (V_b - R_s I_b)$, then (A8) becomes

$$V \approx V_{jb} - R_s I_r + \left(\frac{Z_j}{Z}\right) E_g \ . \tag{A10}$$

Next define

$$v = V - V_{jb} \approx \left(\frac{Z_j}{Z}\right) E_g - R_s I_r \ , \tag{A11}$$

i.e., v will be the excursion of V about the bias point V_{jb}.

Having thus defined v, the next step is to evaluate the current, I. Figure A4 illustrates a nominal non-linear junction V-I characteristic. Since the excursions about the bias point (V_{jb}, I_b) are assumed to be very small, it is again convenient to write the non-linear function as a Taylor series expansion of three terms about the bias point,

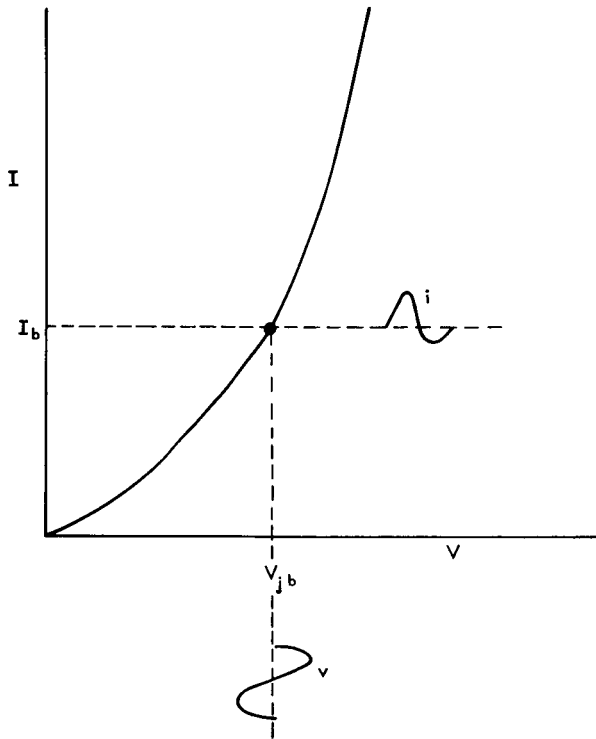$$I = f(V_{jb} + v) \approx f(V_{jb}) + f'(V_{jb}) \cdot v + \frac{1}{2}f''(V_{jb}) \cdot v^2 + \cdots \ . \tag{A12}$$

The first term, $f(V_{jb})$, is simply the bias current I_b. The second term is the linear RF current determined by the differential junction conductance, G, at the bias point,

$$f'(V_{jb}) = \left(\frac{dI}{dV}\right)_{V=V_{jb}} = G = \frac{1}{R}. \tag{A13}$$

In the third term, the second derivative of the function may also be written as the first derivative of the conductance, i.e.,

$$f''(V_{jb}) = \left(\frac{d^2 I}{dV^2}\right)_{V=V_{jb}} = \left(\frac{dG}{dV}\right)_{V=V_{jb}} = G' \tag{A14}$$

Thus, Equation A12 may be written

$$I \approx I_b + Gv + \frac{1}{2} G' v^2. \tag{A15}$$

Figure A4—Nominal V-I characteristic illustration.

The current, I, may now be combined with the current through the condenser, $C\, dv/dt$, to give the current I_g, i.e.,

$$I_g = I + C \frac{dv}{dt} \tag{A16}$$

or

$$I_g \approx I_b + Gv + C \frac{dv}{dt} + \frac{1}{2} G' v^2. \tag{A17}$$

Upon substituting (A2) into (A11), v may be converted into the form

$$v \approx b\left(\frac{Z_j}{Z}\right) e^{j\omega t} - R_s I_r, \tag{A18}$$

and if we now substitute this v into (A17),

$$I_g \approx I_b + (G + j\omega C) b\left(\frac{Z_j}{Z}\right) e^{j\omega t} - GR_s I_r + \frac{1}{2} G' \cdot \left[b\left(\frac{Z_j}{Z}\right) e^{j\omega t} - R_s I_r\right]^2 \tag{A19}$$

30

or

$$I_g \approx I_b - GR_s I_r + \frac{E_g}{Z} + \frac{1}{2} G' \cdot \left[b \left| \frac{Z_j}{Z} \right| e^{j(\omega t + \theta)} - R_s I_r \right]^2.$$ (A20)

Upon equating this I_g to the I_g found in Equation A7, the I_b term and the linear E_g/Z term will drop out, leaving

$$I_r \approx - GR_s I_r + \frac{1}{2} G' \left[b \left| \frac{Z_j}{Z} \right| e^{j(\omega t + \theta)} - R_s I_r \right]^2.$$ (A21)

Only the average value of the squared term is of interest, so that it is necessary to take the real part thereof. Furthermore, the voltage drop $(R_s I_r)$ is very small compared to the RF magnitude of v, i.e.,

$$b \left| \frac{Z_j}{Z} \right| \gg R_s I_r.$$ (A22)

Therefore, $R_s I_r$ can be neglected in the squared term and Equation A21 becomes

$$I_r (1 + GR_s) \approx \frac{1}{2} G' \left[b \left| \frac{Z_j}{Z} \right| \cos(\omega t + \theta) \right]^2,$$ (A23)

from which the average value is obtained to arrive at the rectified current,

$$I_r \sim \frac{G' b^2 |Z_j|^2}{4(1 + GR_s) |Z|^2}.$$ (A24)

In Figure A3, if the resistance R_g is derived entirely from the generator source impedance,* then the incident RF power may be expressed in terms of E_g as

$$P_i = \frac{1}{2} \cdot \frac{|E_g|^2}{4R_g} = \frac{b^2}{8 R_g}.$$ (A25)

Upon dividing Equation A24 by Equation A25, the expression for the rectification current sensitivity, β, is obtained,

$$\beta = \frac{I_r}{P_i} \sim \frac{2G' R_g |Z_j|^2}{(1 + GR_s) |Z|^2}$$ (A26)

_____

*If R_g includes resistance other than from the generator, then a loss correction must be calculated.

Appendix B

Tunnel Diode V-I Characteristic

The voltage-current characteristic of a tunnel diode has not been rigorously derived as yet, so that no single equation is known that is capable of accurately predicting the entire curve (References 15, 16, and 17). However, a reasonably accurate piecewise approximation can be obtained by curve-fitting with an exponential function of the type derived in Nergaard and Glicksman (Reference 15) for an assumed tunnel diode model,

$$I = 2.44 \, I_p \, (\alpha V)^{1.5} \, e^{\alpha V} \quad , \tag{B1}$$

where

$$\alpha = \frac{q}{KT} = \frac{1.6 \cdot 10^{-19} \text{ coulombs}}{4 \cdot 10^{-21} \text{ watts/cycle}}$$

I_p = peak current

V = voltage across diode junction.

For curve-fitting, it is desirable to utilize the general form of Equation B1, together with its first two derivatives,

$$I = A(\alpha V)^\gamma e^{\alpha V} \tag{B2}$$

$$\frac{dI}{dV} = I\left(\frac{\gamma}{V} + \alpha\right) = G \tag{B3}$$

$$\frac{d^2 I}{dV^2} = I\left[\alpha^2 + \frac{2\alpha\gamma}{V} + \frac{\gamma(\gamma-1)}{V^2}\right] = G'. \tag{B4}$$

It will be noted in Equation B3 that the first derivative is the junction conductance, G, of the diode, and in B4 that the second derivative is therefore G'.

The above relationships apply only to the diode junction, so that it is necessary to add a fourth equation in order to account for the series resistance, R_s,

$$V_b = V + I R_s \quad , \tag{B5}$$

where V_b now represents the external voltage across the diode terminals. The value of R_s must be known accurately not only because of its effect upon the V-I characteristic but, also because of its effect upon the microwave performance of the diode. R_s is usually provided as part of the manufacturer's data on the diode but, if it is not known or is in question, then it may be determined from I-V_b slope measurements under forward bias conditions. The necessary relationship is readily obtained by differentiating Equation B5,

$$\frac{dV_b}{dI} = \frac{dV}{dI} + R_s = \frac{1}{\left(\frac{dI}{dV}\right)} + R_s \cdot \tag{B6}$$

Substituting for (dI/dV) from Equation B3 then results in

$$\frac{dV_b}{dI} = \frac{1}{\left(\frac{\gamma}{V} + \alpha\right)} \cdot \left(\frac{1}{I}\right) + R_s \cdot \tag{B7}$$

If the forward bias voltage is large enough to obtain the condition $\gamma/V \ll \alpha$, then Equation B7 simplifies to

$$\frac{dV_b}{dI} = \frac{1}{\alpha I} + R_s, \text{ for } \frac{\gamma}{V} \ll \alpha \tag{B8}$$

which is a straight-line graph of (dV_b/dI) versus $(1/I)$ with R_s given by the intersection of the straight line with the (dV_b/dI) axis. Figure B1 illustrates such a graph plotted for the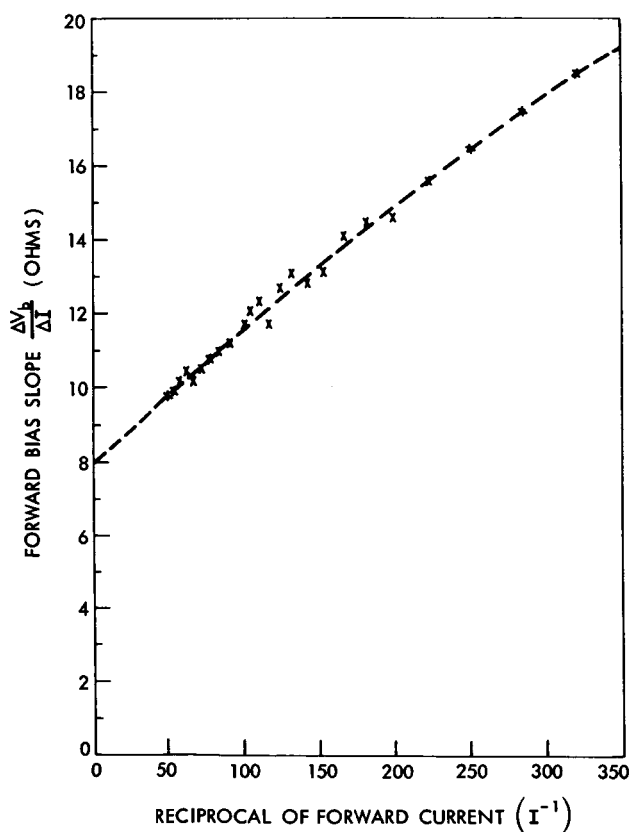 example diode where it will be noted that R_s is 8 ohms. The forward current becomes relatively large during this measurement, so that it is necessary to utilize pulses of low duty cycle in order to prevent heating of the diode junction.

In curve-fitting the forward characteristic of the diode, it has been found that satisfactory accuracy may be obtained by utilizing the I-V_b slope measured at zero bias, plus the reverse bias peak current point values of I_p, V_{bp}. The zero bias slope, G_{d0}, is finite and requires a current component I_1, for which the value of γ in Equation B2 is unity,

$$I_1 = A_1 (\alpha_1 V) e^{\alpha_1 V} , \tag{B9}$$

$$\frac{dI_1}{dV} = G_1 = A_1 \alpha_1 e^{\alpha_1 V} + \alpha_1 I_1 , \tag{B10}$$

and

$$\left. \frac{dI_1}{dV} \right|_{V=0} = G_0 = A_1 \alpha_1 . \tag{B11}$$

Figure B1—Data plot of $(\Delta V_b/\Delta I)$ vs. $(1/I)$ to find R_s

At the peak current point, G_1 must go to zero so that from (B9) and (B10) we obtain,

$$\left.\frac{dI_1}{dV}\right|_{V=V_p} = 0 = I_{p1}\left(\frac{1}{V_p} + \alpha_1\right)$$

or

$$\alpha_1 = \frac{1}{-V_p} \quad . \tag{B12}$$

V_p can be obtained from Equation B5,

$$V_p = V_{bp} - I_p R_s \quad , \tag{B13}$$

so that α_1 is determined. Then A_1 is evaluated from Equation B11. Utilizing the MS-1012 diode as an example, the following values were measured:

$$R_s = 8\,\Omega$$
$$I_p = -0.285\,\text{ma}$$
$$V_{bp} = -0.0483\,\text{volts}$$
$$\text{and} \quad G_{do} = 0.0133\,\text{mhos} .$$

Then from Equation B13 we obtain

$$V_p = -0.0483 + 0.000286 \cdot 8$$
$$\text{and} \quad V_p = -0.046 \quad ,$$

from Equation B12

$$\alpha_1 = \frac{1}{0.046} = 21.75 \quad ,$$

$$R_0 + R_s = R_{do} = \frac{1}{G_{do}} = \frac{1}{0.0133} = 75\,\Omega \quad , \tag{B14}$$

or

$$R_0 = 75 - 8 = 67\,\Omega = \frac{1}{G_0} \quad ,$$

and from Equation B11

$$A_1 = \frac{G_0}{\alpha_1} = \frac{1}{21.75 \cdot 67} = 0.687$$

The calculated I_1 vs. V_b characteristic is shown in comparison with the measured data in Figure B2. Its accuracy holds within 4 percent of the measured data for forward bias up to about 40 milli-volts and for reverse bias to about -8 millivolts. Therefore, the I_1 equation is satisfactory for
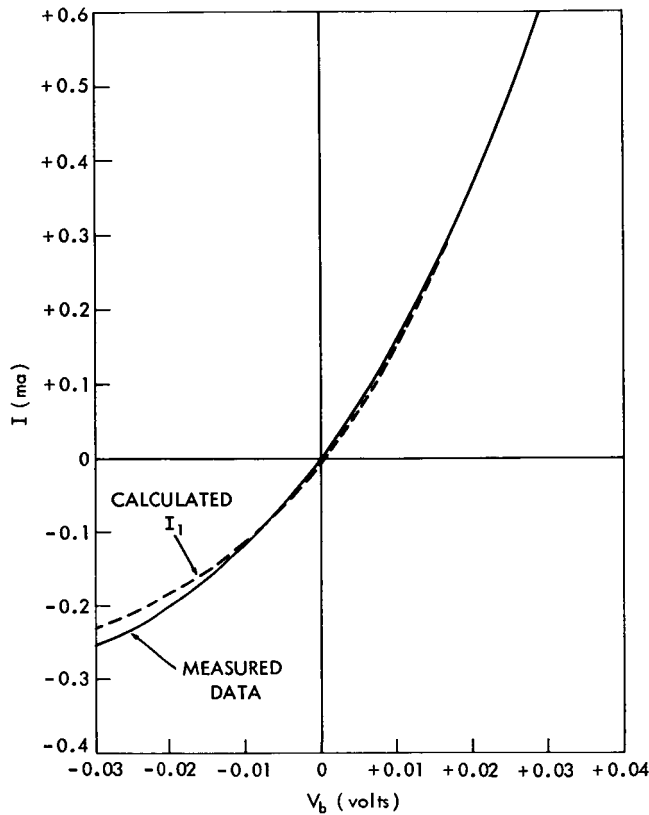
Figure B2—Comparison of calculated current I_1 vs. measured data for example diode.

calculating first and second derivatives under limited forward bias conditions and in the vicinity of zero bias.

Under reverse bias conditions beyond -10 millivolts, current I_1 is not quite accurate enough. For instance, upon substituting Equation B12 into B9 the peak current I_{p1} will be found to be

$$I_{p1} = -\frac{A_1}{e} = \frac{-A_1}{2.718} = \frac{-0.0687}{2.718} = -0.253 \text{ ma}, \quad \text{(B15)}$$

whereas the measured value is -0.286 ma, resulting in an error of 11.5% in I_{p1}. Also, the I_1 equation results in excessive derivative errors near the inflection point, such that it is desirable to either add a second current component based upon $\gamma = 1.5$, or utilize a single equation with an intermediate value of γ. The latter approach results in greatest simplicity.

A single equation curve fit of the negative characteristic is best accomplished by utilizing the inflection point data together with V_p. At the inflection point the second derivative must vanish, so that from Equation B4 one obtains

$$\left.\frac{d^2 I}{dV^2}\right|_{V=V_i} = \alpha^2 I_i \left[1 + \frac{2\gamma}{\alpha V_i} + \frac{\gamma(\gamma-1)}{(\alpha V_i)^2} \right] = 0 \quad , \quad \text{(B16)}$$

which has the solution

$$\alpha V_i = -(\gamma + \sqrt{\gamma}). \quad \text{(B17)}$$

Upon substituting the peak current condition obtained from setting Equation B3 equal to zero,

$$\left.\frac{dI}{dV}\right|_{V=V_p} = 0 = I_p \left(\frac{\gamma}{V_p} + \alpha \right)$$

or

$$\text{(B18)}$$

$$\alpha = \frac{\gamma}{-V_p} \quad .$$

Then Equation B17 may be written as

$$V_i = V_p \left(1 + \frac{1}{\sqrt{\gamma}}\right) . \qquad (B19)$$

By substituting Equations B18 and B19 into Equation B2 one can relate the inflection point current to the peak current,

$$I_i = \frac{\left(1 + \frac{1}{\sqrt{\gamma}}\right)^{\gamma}}{e^{\sqrt{\gamma}}} \cdot I_p . \qquad (B20)$$

The final relationship needed is the slope (conductance) at the inflection point, and this is obtained by substituting Equations B18, B19, and B20 into Equation B3,

$$G_i = I_i \left(\frac{\gamma}{V_i} + a\right) = -\frac{\gamma^{1-\gamma/2} (1 + \sqrt{\gamma})^{\gamma-1}}{e^{\sqrt{\gamma}}} \cdot \frac{I_p}{V_p} , \qquad (B21)$$

which may then be written as,

$$-\frac{\gamma^{1-\gamma/2} (1 + \sqrt{\gamma})^{\gamma-1}}{e^{\sqrt{\gamma}}} = \left(\frac{V_p}{I_p R_i}\right) , \qquad (B22)$$

where R_i is the inflection point negative resistance.

Equation B22 results in the ratio of V_p to $I_p R_i$ as a function of γ only. In curve-fitting to the actual diode characteristic, only three of the five conditions (I_p, V_p, I_i, V_i, R_i) can be satisfied by the three constants available to us in the single Equation B2, so that the remaining two quantities must be compromised. In practice, it has been found that the most satisfactory compromise is obtained by using the measured values of V_p and R_i, and choosing the inflection point to lie on the measured data curve. This throws most of the compromise error into the magnitude of I_p, but the price paid is small. Again utilizing the MS1012 diode as an example, the measured values of V_p and R_i were found to be

$$V_p = -0.046 \quad \text{as determined previously}$$
$$R_{di} = -360 \ \Omega \ \text{measured maximum slope}$$

then

$$R_i = R_{di} - R_s = -360 - 8 = -368 \Omega . \qquad (B23)$$

Knowing V_p and R_i, we can now utilize Equations B20, B22, and B19 to calculate pair values of I_i and V_i for various values of γ. The equation for I_i simplifies to,

$$I_i = -\frac{(1 + \sqrt{\gamma})}{\gamma} \left(\frac{V_p}{R_i}\right) . \qquad (B24)$$

Upon converting V_i into V_{bi} values via the relationship

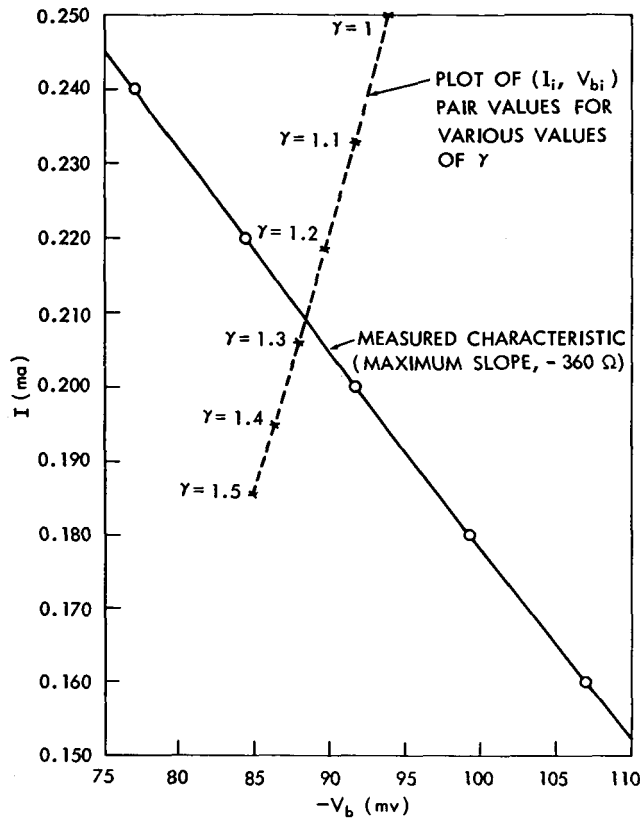$$V_{bi} = V_i + I_i R_s, \qquad (B25)$$

Figure B3—Pair values of (I_i, V_{bi}) plotted on example diode characteristic in order to determine the curve-fitted value for γ.

we then obtain pair values of (I_i, V_{bi}) that can be plotted directly on the measured current-voltage characteristic of the diode to obtain an intersection point as illustrated in Figure B3. The intersection point occurs at an interpolated value of $\gamma = 1.275$. Upon using this value of γ one can calculate the following values from the associated equations:

I_i = -0.209 ma from Equation B24
V_i = -0.0867 volts from Equation B19
V_{bi} = -0.08837 volts from Equation B25
R_i = -368 Ω from Equation B3 and B18
I_p = -0.2875 ma from Equation B20.

The values of I_i, V_{bi}, and R_i show perfect agreement as one would expect, since the curve fitting was performed there. However, note that the calculated value for I_p agrees very closely with the measured peak-current value of -0.286 ma and, in fact, is accurate within the overall measurement accuracy of about 0.5 percent. The calculations by this method of curve fitting are very sensitive to the value of V_p.

Let us identify this portion of the piecewise current approximation by I_2 and evaluate the associated constants of A_2 and α_2. Thus, from (B2) we have

$$I_2 = A_2 (\alpha_2 V)^{\gamma_2} e^{\alpha_2 V} \quad , \tag{B26}$$

where $\gamma_2 = 1.275$ as calculated above

$$\alpha_2 = \frac{\gamma_2}{-V_p} = \frac{1.275}{0.046} = 27.73 \quad \text{from Equation B18.}$$

Upon substituting α_2 and V_p into Equation B26 we get I_{p2}. So

$$I_{p2} = A_2 (-\gamma_2)^{\gamma_2} e^{-\gamma_2} = A_2 \left(\frac{-\gamma_2}{e}\right)^{\gamma_2} \tag{B27}$$

and

$$A_2 = I_{p2} \left(\frac{e}{-\gamma_2}\right)^{\gamma_2} = +2.626 \cdot 0.2875 = 0.755 \text{ ma.} \tag{B28}$$

The calculated I_2 vs. V_b characteristic is shown in Figure B4 in comparison with measured data. It is very accurate in the vicinity of the inflection point, where it was curve fitted, and it holds within 3 percent accuracy of the measured data for reverse bias voltage range of approximately -20 to -130 millivolts. Beyond -130 millivolts the "valley region" of the diode characteristic commences and leads into the reverse voltage breakdown, so that I_2 accuracy becomes progressively worse. The accuracy also deteriorates as one approaches zero bias, and continues to be poor for forward bias. Therefore, the I_2 equation is satisfactory for calculating first and second derivatives under reverse bias conditions only, and it should be restricted to the range of approximately -10 to -150 millivolts.
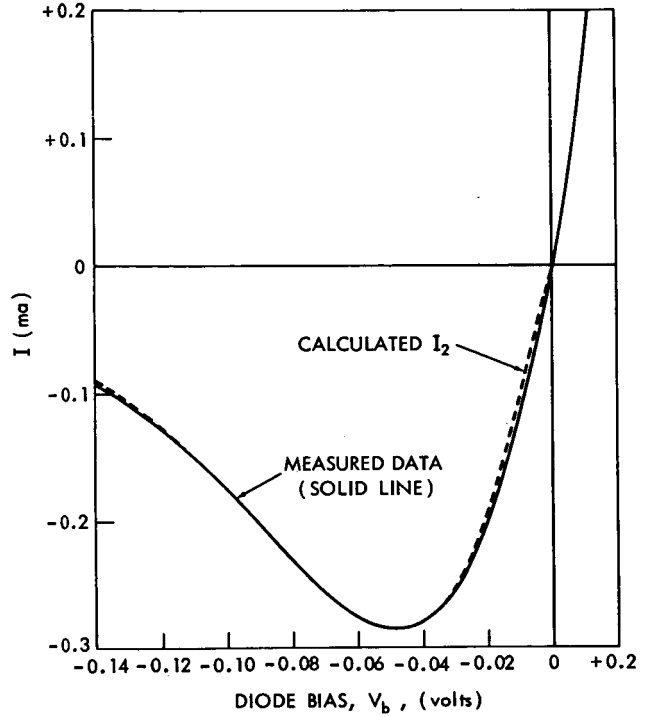

Figure B4—Comparison of calculated current I_2 vs. measured data for example diode.

Appendix C

Symbols and Definitions

A   -   constant in diode current equation, Appendix B

b   -   amplitude of E_g

B_v -   video bandwidth

C   -   diode junction capacitance

C_b -   rf by-pass condenser

C_v -   total video shunt capacitance

C_p -   diode package and mounting capacitance

E_g -   series equivalent rf signal generator voltage

$\sqrt{E_n^2}$ -   total r.m.s. noise voltage

f   -   rf frequency

f_c -   diode cut-off frequency for positive R

f_r -   diode resistive cut-off frequency for negative R

Δf -   rf bandwidth

G   -   diode differential junction conductance, (dI/dV)

G'   -   first derivative of G

I   -   resistive component of diode junction current

I_b -   diode dc bias current

I_g -   total diode current, $(I_g = I + C (dV/dt))$

I_p -   tunnel diode peak point current value

I_i -   tunnel diode inflection point current value

I_r -   detector rectified output current

41

I_{eq} – equivalent shot-noise-producing dc current

$\sqrt{I_n^2}$ – total r.m.s. noise current due to diode and R_v

k – Boltzmann's constant, $(1.38 \cdot 10^{-16}$ ergs/degree Kelvin$)$

L – equivalent rf circuit series inductance plus L_s

L_s – diode series inductance

M – diode figure of merit

P_i – rf power incident upon the detector

P_t – tangential sensitivity input rf power level

q – electronic charge, $(1.6 \cdot 10^{-20}$ coulombs$)$

Q – circuit Q factor

R – diode differential junction resistance, (dV/dI)

R_g – equivalent series resistance of rf circuit

R_s – diode series resistance

R_v – equivalent video circuit resistance

R_i – total equivalent resistance of diode in parallel with R_v (Note: R_i is also used in Appendix B to denote the inflection point negative resistance value of R)

R_{eq} – amplifier excess noise equivalent resistor

r – series equivalent junction resistance of diode

r_0 – value of r at ω_0

T – temperature in degrees Kelvin

V – diode junction voltage

V_b – diode dc bias voltage

V_{jb} – junction dc bias voltage, $(V_{jb} = V_b - I_b R_s)$

v – excursion of V from V_{jb}, $(v = V - V_{jb})$

Z – total equivalent series impedance of diode plus rf circuit

Z_j – equivalent series impedance of diode junction

α - constant in diode current equation, Appendix B

β - rectification current sensitivity

γ - constant in diode current equation, Appendix B

Γ - reflection coefficient referred to R_g

τ - pulse rise time between 10 and 90 percent amplitude points

ω - frequency in radians per second

ω_0 - value of ω at center of rf passband

Subscripts:

0 - refers to diode zero bias point except for r_0, ω_0, β_0, Γ_0

p - refers to diode peak current bias point

i - refers to diode inflection bias point except for the special case noted for R_i